Influence of deep-water derived isoprenoid tetraether lipids on the TEX_{86}^H paleothermometer in the Mediterranean Sea

Jung-Hyun Kim [a,*], Stefan Schouten [a,b], Marta Rodrigo-Gámiz [a],
Sebastiaan Rampen [a,b], Gianluca Marino [b,1], Carme Huguet [a,2], Peer Helmke [c],
Roselyne Buscail [d], Ellen C. Hopmans [a], Jörg Pross [e], Francesca Sangiorgi [b],
Jack B.M. Middelburg [b], Jaap S. Sinninghe Damsté [a,b]

[a] *NIOZ Royal Netherlands Institute for Sea Research, NL-1790 AB Den Burg, The Netherlands*
[b] *University of Utrecht, Faculty of Geosciences, P.O. Box 80.021, NL-3508 TA Utrecht, The Netherlands*
[c] *Federal Institute of Hydrology, Department M4: "Geo-Information and Remote Sensing, GRDC", Am Mainzer Tor,*
D-56068 Koblenz, Germany
[d] *CEFREM-UMR CNRS 5110-University of Perpignan, 52 Avenue Paul Alduy, F-66860 Perpignan, France*
[e] *Paleoenvironmental Dynamics Group, University of Heidelberg, Institute of Earth Sciences, Im Neuenheimer Feld 234,*
D-69120 Heidelberg, Germany

Abstract

The TEX_{86}^H paleothermometer based on isoprenoid glycerol dialkyl glycerol tetraethers (isoGDGTs) has widely been applied in various marine settings to reconstruct past sea surface temperatures (SSTs). However, it still remains uncertain how well this proxy reconstructs annual mean SSTs. Here, we assess environmental factors governing the TEX_{86}^H paleothermometer in the Mediterranean Sea, by studying the distribution of isoGDGTs in surface sediments, suspended particulate matter (SPM), and two sediment cores. A redundancy analysis using the fractional abundance of the six major isoGDGTs indicates that the sedimentary isoGDGTs are mostly influenced by three environmental factors explaining a large part (74%) of the variance in isoGDGT distribution. In order of decreasing significance, these factors are annual mean SST, continental organic matter input as indicated by the BIT index, and water depth. However, when considering only the four isoGDGTs that are used for the TEX_{86}^H proxy, water depth is the most significant parameter, explaining 63% of the variance. Indeed, a strong positive relationship between water depth and TEX_{86}^H is observed in both surface sediments and SPM from the Mediterranean Sea. This is driven by an increase in fractional abundances of GDGT-2 and crenarchaeol regio-isomer and a decrease in the fractional abundances of GDGT-1 and GDGT-3 with increasing water depth, leading to a bias to higher temperatures of TEX_{86}^H in deep-water surface sediments. The fact that the water-depth trend is also apparent in SPM suggests that this change might be due to a change in thaumarchaeotal community thriving below surface mixed-layer waters and that this signal is, at least partly, incorporated into sedimentary isoGDGTs. Interestingly, surface-sediment TEX_{86}^H values from >1000 m water depth do not show a correlation with water depth anymore and instead are correlated to annual mean SSTs. A composite deep-water TEX_{86}^H dataset of surface sediments from both the Mediterranean Sea and the Red Sea, interconnected regional restricted basins with relatively high bottom-water temperatures and high salinity, forms a distinctive correlation line, statistically distinct from that of the general global correlation. Application of this correlation on two sedimentary

---

* Corresponding author. Tel.: +31 (0)222 369567; fax: +31 (0)222 319674.
E-mail address: Jung-Hyun.Kim@nioz.nl (J.-H. Kim).
[1] Present address: Research School of Earth Sciences, The Australian National University, Canberra, ACT 0200, Australia.
[2] Present address: Universitat Autònoma de Barcelona (UAB), Institut de Ciència i Tecnologia Ambientals (ICTA), Bellaterra (Cerdanyola), Spain.

records from the western Mediterranean Sea covering the last deglaciation yields SSTs nearly identical to those obtained with the $U_{37}^{K'}$ paleothermometer, whereas the global calibration substantially overestimates SSTs. Our results show that the warm bias of the TEX_{86}^H proxy in the Mediterranean Sea is not due to seasonality, as previously suggested. Further research is needed to elucidate the mechanism behind the strong water depth trend of TEX_{86}^H in the Mediterranean Sea which is not apparent in open ocean settings.

1. INTRODUCTION

Thaumarchaeota, formerly known as Group I Crenarchaeota (e.g., Brochier-Armanet et al., 2008; Spang et al., 2010), produce membrane-spanning isoprenoid glycerol dialkyl glycerol tetraethers (isoGDGTs). There are different types of isoGDGTs containing 0 to 3 cyclopentane moieties (GDGT-0 to GDGT-3; Fig. 1) and crenarchaeol, which in addition to 4 cyclopentane moieties has a cyclohexane moiety (Schouten et al., 2000; Sinninghe Damsté et al., 2002). Relatively small quantities of a regio-isomer of crenarchaeol are also biosynthesized. Schouten et al. (2002) found that the number of cyclopentane moieties in marine sediments increased with rising sea surface temperatures (SSTs) and introduced the TEX_{86} (TetraEther indeX of tetraethers consisting of 86 carbon atoms) as a SST proxy. Subsequently, this proxy has slightly been modified as TEX_{86}^H, i.e., defined as the logarithmic function of TEX_{86}, for (sub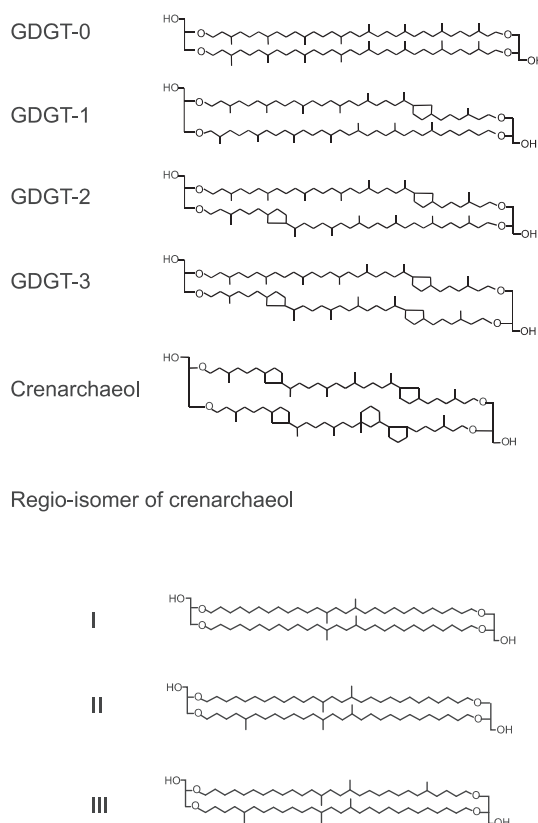)tropical oceans and greenhouse periods, and as TEX_{86}^L, with a logarithmic function that does not include the crenarchaeol regio-isomer, for (sub)polar oceans (Kim et al., 2010a). On a global scale, both TEX_{86}^H and TEX_{86}^L correlate well with annual mean SSTs (Kim et al. 2010a) as well as with depth-integrated annual mean temperatures from 0 to 200 m water depth (Kim et al., 2012a,b). Mesocosm experiments confirmed that Thaumarchaeota changed their membrane composition with growth temperature and showed that changes in salinity and nutrients do not substantially affect the temperature signal (Wuchter et al., 2004; Schouten et al., 2007a).

Although applications of the isoGDGT-based temperature proxies in various marine sediment core sites have shown their potential, especially where the application of other proxies was limited (e.g., Schouten et al., 2003; Liu et al., 2009; Littler et al., 2011; Bijl et al., 2013), it still remains uncertain how well these proxies reconstruct annual mean SSTs due to several complicating factors (Pearson and Ingalls, 2013; Schouten et al., 2013 and references therein). In particular, it has been shown that Thaumarchaeota, the major producer of the isoGDGT membrane lipids in the marine water-column, are not light-dependent as they use ammonia as their energy source, i.e., they are chemoautotrophs (e.g., Wuchter et al., 2003; Herndl et al., 2005; Könneke et al., 2005). Hence, they occur throughout the water-column (e.g., Karner et al., 2001; Herndl et al., 2005) and in the underlying sediments (e.g., Francis et al., 2005; Dang et al., 2013). Several studies for both modern conditions (e.g., Huguet et al., 2007; Lee et al., 2008; Jia et al., 2012) and paleoenvironments (e.g., Lopes dos Santos et al., 2010; Kim et al., 2012a,b) have actually shown that isoGDGT-based temperature proxies in some regions may better reflect subsurface temperatures (ca. 30–200 m water depth) rather than annual mean SSTs (upper mixed layer of ca. 30 m). Furthermore, the $\Delta^{14}C$ of isoGDGTs have demonstrated that the deep-water residing Thaumarchaeota, i.e., below the euphotic zone, may have the potential to substantially contribute to sedimentary isoGDGTs (Pearson et al., 2001; Smittenberg et al., 2004; Ingalls et al., 2006; Shah et al., 2008). Recently, Taylor et al. (2013) have suggested that Thaumarchaeota thriving in the deeper, bathypelagic water-column (>1000 m water depth) are responsible for increased contributions of GDGT-2 over GDGT-3 to sedimentary isoGDGTs. Consequently, they have argued that the contribution of deep-water derived isoGDGTs may cause a warm bias of isoGDGT-based temperature proxies. Therefore, it is timely to constrain other environmental factors rather than just annual mean SSTs that control isoGDGT distributions and thus influence the isoGDGT-based temperature proxies.

GDGT-0

GDGT-1

GDGT-2

GDGT-3

Crenarchaeol

Regio-isomer of crenarchaeol

I

II

III

Fig. 1. Structures of isoprenoid and branched GDGTs used in this study.

The Mediterranean Sea is a marginal, landlocked sea and shows a rapid and amplified response to climate changes (e.g., Rohling et al., 2002; Kotthoff et al., 2008; Marino et al., 2009). Some previous studies in this region showed that TEX_{86}^H-derived SSTs were generally higher than those of $U_{37}^{K'}$, an organic-based SST proxy based on the ratio of long-chain diunsaturated and triunsaturated alkenones produced by Haptophyte algae (Brassell et al., 1986; Prahl and Wakeham, 1987), likely because the TEX_{86}^H record was predominantly skewed toward reconstructed temperatures warmer than annual mean SSTs (Castañeda et al., 2010; Leider et al., 2010; Huguet et al., 2011; Grauel et al., 2013; Nieto-Moreno et al., 2013). In contrast, Menzel et al. (2006) showed that $U_{37}^{K'}$-based SSTs were virtually constant while TEX_{86}-based SST estimates decreased substantially during Pliocene sapropel deposition, an interval of strong (upper) water-column stratification. They attributed the difference to Thaumarchaeota thriving at depths corresponding to the deep and cold chemocline. Hence, it appears that the Mediterranean Sea is an ideal test-bed to assess whether environmental factors other than annual mean SST control the TEX_{86}^H paleothermometer.

In this study, we investigated a large number of new core-top samples ($n = 146$) and six suspended particulate matter (SPM) samples collected from shallow- and deep-water masses at three different stations in the Mediterranean Sea. In addition, we analyzed two gravity cores from the Alboran Sea, the westernmost Mediterranean Sea, which cover the last 20 kyr (thousand years) (Rodrigo-Gámiz et al., 2014). Based on the integration of these new data with previously published data, we assess the influence of environmental factors such as SSTs, continental-derived organic matter input, water depth, and primary productivity on the isoGDGT distributions. Our study sheds light on applicability of the TEX_{86}^H paleothermometer in the Mediterranean Sea and potentially other deep restricted basins.

2. MATERIAL AND METHODS

2.1. Sample collection and environmental data acquisition

Mediterranean core-tops analyzed in this study ($n = 146$) were mostly collected using box- and multi-corers from a variety of locations and different water depths (Fig. 2, Appendix 1). They represent the uppermost surface sediments with a depth from 0 to 2 cm. The core-top samples from the Gulf of Lions were retrieved through several French (River dominated Ocean Margins) and international (European Margin Strata Formation and Hotspot Ecosystem Research on the Margins of European Seas) research programs. The samples from the Balearic Sea were collected at sites situated northwest of Balearic Island and southwest of Mallorca Island during the cruise IDEA with R/V Garcia del Cid in 2004 and the rest of the samples during the R/V Meteor cruise M51/3 in 2001.

Six SPM samples were taken at three different stations during the Bonifacio2011 and MAMBA_C 2011 cruises with R/V URANIA between 14 and 29 March 2011 and between 9 and 22 September 2011, respectively (Fig. 2, Appendix 2). They were collected at water depths of 50 m and 2000–3000 m (Fig. 2). To collect SPM, 170 to 240 L of water at 50 m water depth and 3400 to 5000 L of water at 2000–3000 m water depths were filtered over ashed glass-fiber filters (Whatman GF-F, 0.7 μm pore size, 142 mm diameter) with a McLane in-situ pump system (WTS 6-1-142LV, McLane Labs, Falmouth, MA) installed in a conductivity, temperature, and depth (CTD) rosette frame. Even though the nominal pore size of the filters is larger than thaumarchaeotal cells (typically <0.6 μm; Könneke et al., 2005), previous studies have shown that the concentration profiles of isoGDGTs obtained from 0.7 μm filters correspond well with those of thaumarchaeotal DNA obtained from 0.2 μm filters and that isoGDGT distributions are likely representative (e.g., Herfort et al., 2007; Schouten et al., 2012).

We also analyzed two gravity cores 434G and 293G (Fig. 2A). Core 434G (252.5 cm long; Rodrigo-Gámiz et al., 2014) was retrieved in the West Alboran Sea (36°12.313 N, 4°18.735 W; 1108 m water depth) during the Training Through Research (TTR) 17 cruise with the R/V Professor Logachev. Core 293G (402 cm long; Rodrigo-Gámiz et al., 2014) was recovered from the East Alboran Sea (36°10.414 N, 2°45.280 W; 1840 m water depth) during the TTR 12 cruise with the R/V Professor Logachev.

Following the study by Kim et al. (2010a), SST data for each core-top sampling site were retrieved from the NSIPP (NASA Seasonal-to-Interannual Prediction Project) AVHRR (Advanced Very High Resolution Radiometer) 9.28 km resolution monthly Pathfinder + Erosion SST climatology dataset for the period of 1985 to 1995 from the Physical Oceanography Distributed Active Archive Center at NASA Jet Propulsion Laboratory, Pasadena, CA (Casey and Cornillon, 1999). We used 10-yr average values of the annual mean climatology SST data to explore the relationship of the isoGDGT distributions with SSTs. In addition, annual mean temperatures from different water depths were obtained from the World Ocean Atlas 13 (WOA13) dataset (Locarnini et al., 2013). Depth-weighted annual mean temperatures from 0 to 200 m water depth were calculated following to the approach by Kim et al. (2008).

Primary productivity data used were monthly mean sets of the vertically generalized production model data (Behrenfeld and Falkowski, 1997) retrieved from Oregon State University (site: http://www.science.oregonstate.edu/ocean.productivity/index.php).

2.2. Lipid extraction and purification procedure

Core-top and down-core sediments (1–5 g) were freeze-dried and homogenized with a mortar and a pestle. The sediments were extracted by Dionex™ accelerated solvent extraction (DIONEX ASE 200) using a mixture of dichloromethane (DCM):methanol (MeOH) (9:1, v:v) at a temperature of 100 °C and a pressure of 7.6×10^6 Pa. The supernatants were combined, the solvents were removed by rotary evaporation, and the extracts were taken up in DCM and blown down under a stream of nitrogen.

Freeze-dried SPM samples were first saponified by refluxing for 1 h with 1 M KOH in MeOH (96%). After
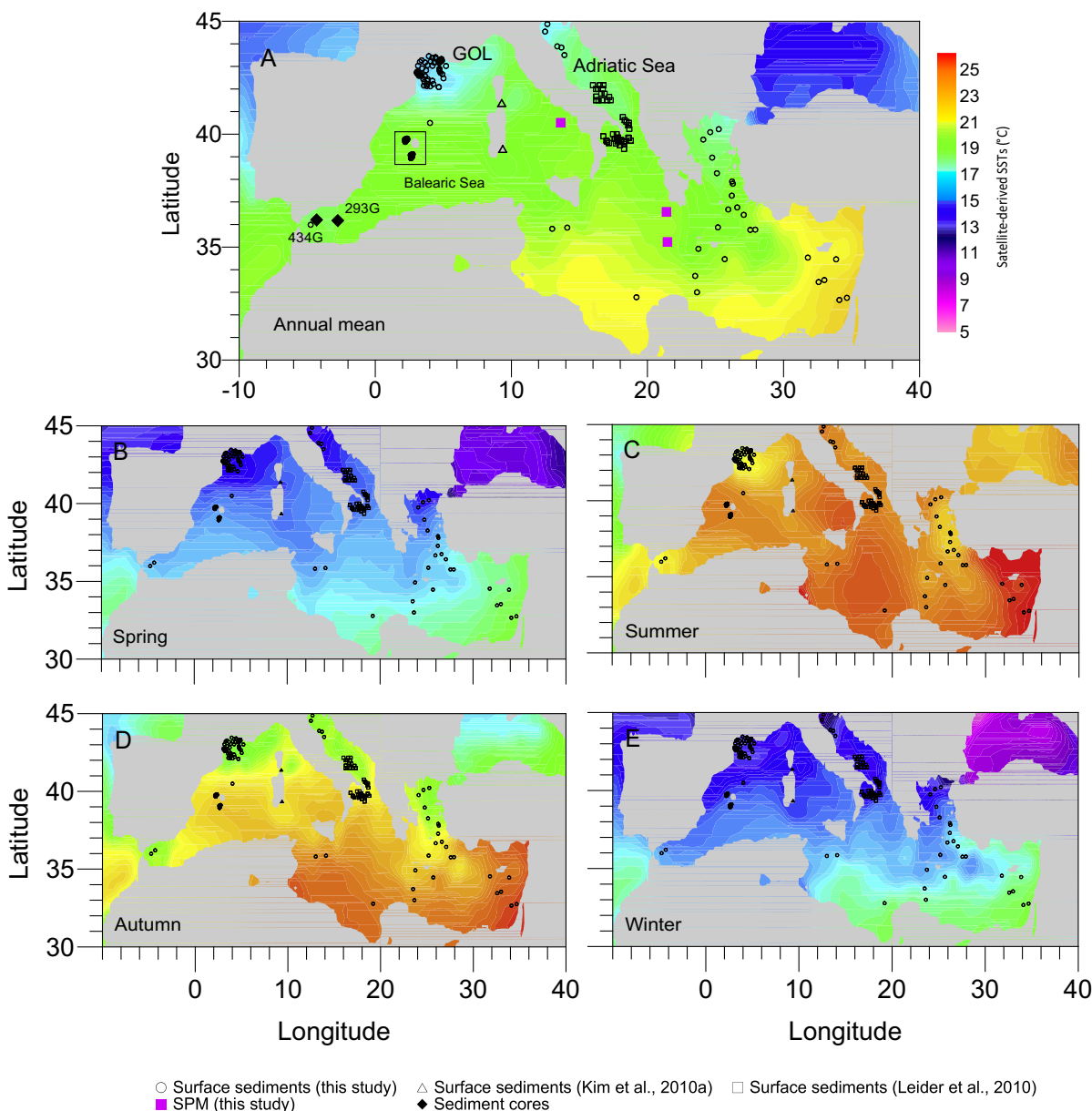
Fig. 2. Spatial distribution pattern of the 10-yr average satellite-derived SSTs in the Mediterranean Sea (based on data from Casey and Cornillon, 1999): (A) annual mean, (B) spring (March–May), (C) summer (June–August), (D) autumn (September–November), and (E) winter (December–February). Black open circles indicate newly analyzed core-tops in this study and open triangles and squares show the positions of the core-tops previously analyzed by Kim et al. (2010a) and Leider et al. (2010), respectively. Three filled purple squares indicate the SPM sampling sites. Two filled diamonds show the sediment core positions (cores 434G and 293G) considered in this study. GOL indicates the Gulf of Lions. (For interpretation of the references to colour in this figure legend, the reader is referred to the web version of this article.)

cooling, solvents were neutralized using 4 M HCl:MeOH (1:1, v:v) and transferred to separatory funnels containing bidistilled H$_2$O. Subsequently, filters were extracted using MeOH:H$_2$O (1:1, v:v), MeOH, and DCM (3×) and all solvents were collected in the separatory funnels. The DCM layers were separated from the H$_2$O:MeOH layers and the remaining H$_2$O:MeOH layers were extracted (3×) with DCM. The DCM extracts were combined for the different samples, and rotary evaporated to near dryness. Thereafter, both filters and obtained extracts were saponified again, this time by refluxing for 3 h with 4 M HCl:MeOH (1:1,

v:v). After cooling, the solvents were neutralized using 1 M KOH. For the saponified filters, the solvents were again transferred to separatory funnels containing bidistilled H$_2$O. Subsequently, filters were extracted using MeOH:H$_2$O (1:1, v:v), MeOH, and DCM (3×) and all solvents were collected in the separatory funnels. The DCM layers were separated from the H$_2$O:MeOH layers and the remaining H$_2$O:MeOH layers were extracted (3×) with DCM. The DCM extracts were combined for the different samples and rotary evaporated to near dryness. For the saponified extracts, bidistilled H$_2$O was added and the

H_2O:MeOH layers were extracted (4×) with DCM. All extracts were combined for the different samples, eluted in DCM over pipette-columns containing Na_2SO_4 to remove remaining salts and H_2O, and dried under N_2.

The total extracts were separated by Al_2O_3 column chromatography using hexane:DCM (9:1, v:v), hexane:DCM (1:1, v:v), and DCM:MeOH (1:1, v:v) as subsequent eluents. The polar (DCM:MeOH) fractions were concentrated under N_2, dissolved in hexane:propanol (99:1, v:v), and filtered using a 0.4 μm PTFE filter prior to injection.

2.3. GDGT analysis and temperature estimation

All GDGT analyses were conducted at NIOZ. The filtered polar fractions were analyzed using high performance liquid chromatography/atmospheric pressure positive ion chemical ionization-mass spectrometry (Agilent Technologies 1100 series, Palo-Alto, CA, USA) equipped with an auto-injector and Chemstation chromatography manager software. Separation was achieved on a Prevail Cyano column (2.1 × 150 mm, 3 μm; Alltech, Deerfield, IL, USA), maintained at 30 °C. Injection volumes varied from 1 to 20 μl. GDGTs were eluted isocratically with 99% A and 1% B for 5 min, followed by a linear gradient to 1.8% B in 45 min, where A = hexane and B = propanol. Flow rate was 0.2 ml min^{-1}. After each analysis the column was cleaned by back-flushing hexane:propanol (90:10, v:v) at 0.2 ml min^{-1} for 10 min. GDGTs were detected by single ion monitoring of their [M+H]$^+$ ions (dwell time 237 ms) (Schouten et al., 2007b). Fractional abundances of each iso-GDGT component were obtained by normalizing each peak area to the summed area of all six isoGDGTs.

The TEX$_{86}^H$ (Kim et al., 2010a) and the BIT (Branched and Isoprenoid Tetraether) index (Hopmans et al., 2004), a proxy for input of continental-derived GDGTs were calculated as follows:

$$TEX_{86}^H = log\left(\frac{[GDGT\text{-}2] + [GDGT\text{-}3] + [Cren']}{[GDGT\text{-}1] + [GDGT\text{-}2] + [GDGT\text{-}3] + [Cren']}\right)$$
$$= log(TEX_{86}) \qquad (1)$$

$$BIT\ index = \frac{[I] + [II] + [III]}{[I] + [II] + [III] + [Cren]} \qquad (2)$$

GDGT-1, GDGT-2, and GDGT-3 indicate isoGDGTs containing 1, 2, and 3 cyclopentane moieties, respectively (Fig. 1). The roman numerals (I, II, and III) refer to branched GDGTs while Cren and Cren' indicate crenarchaeol and its regio-isomer, respectively (Fig. 1). TEX$_{86}^H$ values were converted into temperature values using the global core-top calibration for satellite-derived annual mean SST (Eq. (3), Kim et al., 2010a):

$$T = 68.4 \times TEX_{86}^H + 38.6 \ (r^2 = 0.87, \ n = 255,$$
$$p < 0.0001, 0\ m\ water\ depth) \qquad (3)$$

2.4. Statistical analysis

To examine the relationship between TEX$_{86}^H$ and temperature among different datasets, the homogeneity of slopes and the difference in intercept were tested with an analysis of covariance (ANCOVA). Principal component analysis (PCA) was performed on the fractional abundances of iso-GDGTs to provide a general view of the variability within the distribution of isoGDGTs. Fractional abundances of each isoGDGT component were obtained by normalizing each peak area to the summed area of all isoGDGTs considered. The relationships between isoGDGTs and environmental variables such as SST (annual mean, spring, summer, autumn, and winter), primary productivity (annual mean, spring, summer, autumn, and winter), water depth, and BIT (an indicator of continental-derived organic matter input) were assessed by applying redundancy analysis (RDA). Multicollinearity between environmental variables was examined using variance inflation factors (VIFs). Large VIFs (>150) indicate that a variable is highly correlated with other variables, and thus contributes little information to the ordination. Preliminary ordinations revealed that annual mean primary productivity had a high VIF value. Therefore, this variable was excluded in the RDA. All statistical analyses were performed using the R-3.0.1 packages.

3. RESULTS

3.1. GDGT distributions in surface sediments, SPM, and sediment cores

We analyzed 146 core-tops collected from Alboran Sea ($n = 2$), Balearic Sea ($n = 39$), Gulf of Lions ($n = 72$), Adriatic Sea ($n = 6$), Aegean Sea ($n = 14$), Ionian Sea ($n = 3$), Libyan Sea ($n = 4$), and Levantine Sea ($n = 6$). TEX$_{86}^H$ values ranged from −0.45 to −0.15 (Appendix 1). The reconstructed SSTs varied between 7.7 and 28.6 °C using the global core-top calibration for 0 m water depth (Eq. (3)) from Kim et al. (2010a). TEX$_{86}^H$-derived SSTs strongly deviated from satellite-derived SSTs for annual mean, spring, summer, autumn, and winter seasons (Fig. 3). The difference between TEX$_{86}^H$-derived SST and annual mean temperature (ΔT) ranged from −10 to 9 °C, substantially larger than the error range of the TEX$_{86}^H$ temperature estimates, i.e., ±3 °C, which includes the uncertainty associated with the calibration (±2.5 °C; Kim et al., 2010a) and the analytical error (0.2 °C). The BIT index in surface sediments varied between 0.0 and 0.85, with higher values in the Rhône prodelta (>0.4; Appendix 1).

We also analyzed six SPM samples collected at three different stations in the central Mediterranean Sea (Fig. 2A), three at a water depth of 50 m and three at water depths between 2000 and 3000 m. TEX$_{86}^H$ values varied between −0.19 and −0.17 in the shallow water masses and between −0.12 and −0.11 in the deep-water masses (Appendix 2). The converted temperatures using the global core-top calibration (Eq. (3)) corresponded to an average temperature of 26.3 ± 0.7 °C for the shallow SPM samples and 31.0 ± 0.2 °C for the deep SPM samples. Values for the BIT index were on average 0.01 ± 0.01 for the shallow water SPM and 0.03 ± 0.02 for the deep-water SPM (Appendix 2).

Core 434G had TEX$_{86}^H$ values between −0.32 and −0.18 over the last 14 kyr and core 293G between −0.40 and −0.18 over the last 20 kyr (Appendix 3). When TEX$_{86}^H$ values were translated to SSTs using the global core-top
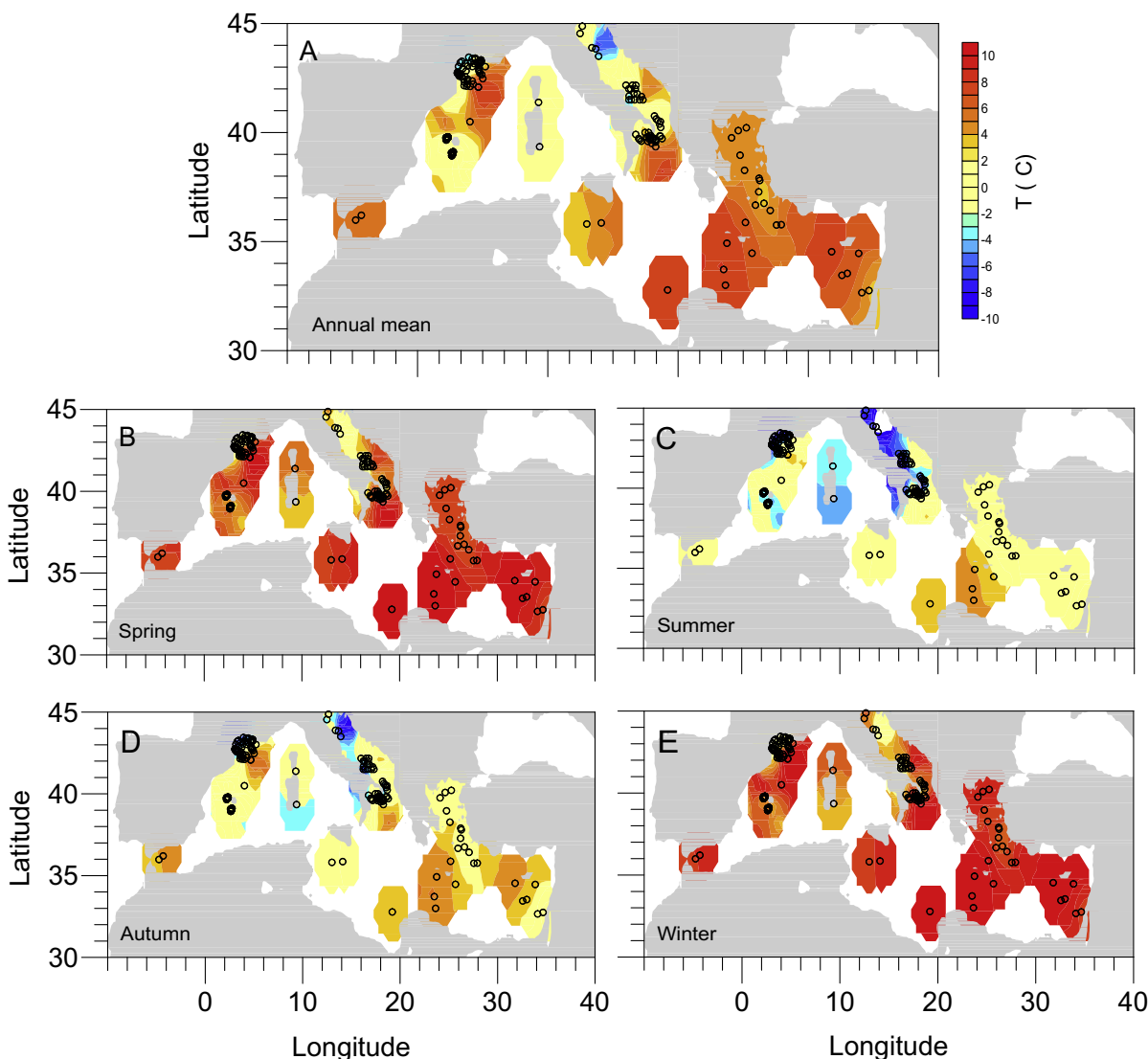
Fig. 3. Temperature differences (ΔT) between TEX_{86}^H-derived temperatures using Eq. (3) and satellite-derived SSTs: (A) annual mean, (B) spring (March–May), (C) summer (June–August), (D) autumn (September–November), and (D) winter (December–February). Black open circles indicate core positions where the TEX_{86}^H data were available in this study. The spatial distribution pattern is based on variogram analysis and ordinary kriging, interpolating the data to a $0.5° \times 0.5°$ grid with $2° \times 2°$ searching radius. (For interpretation of the references to colour in this figure legend, the reader is referred to the web version of this article.)

calibration (Eq. (3)), TEX_{86}^H-derived SSTs ranged from 17 to 26 °C for core 434G and from 11 to 26 °C for core 293G. The BIT index values were low in both cores, varying between 0.01 and 0.04 for core 434G and between 0.01 and 0.17 for core 293G.

3.2. Statistical data treatment of isoGDGT distributions in surface sediments

The newly obtained data for surface sediments were combined with previously published GDGT data from the Tyrrhenian Sea ($n = 2$; Kim et al., 2010a) and the Adriatic Sea ($n = 46$; Leider et al., 2010) to establish a Mediterranean core-top dataset ($n = 194$; see Fig. 2 for all sample locations). An instrumental offset between the data obtained at the NIOZ and those by Leider et al. (2010), although possible,

would likely have minor consequences for the results, as recently shown by a large interlaboratory study of TEX_{86} analysis (Schouten et al., 2014). The comparison of TEX_{86}^H values with annual mean SST using our Mediterranean core-top dataset showed a lower slope of the calibration line and a weaker correlation with considerable scatter ($r^2 = 0.5$, $p < 0.0001$, black line, Fig. 4) than the global core-top correlation of Kim et al. (2010a) ($r^2 = 0.87$, $p < 0.0001$; Fig. 4, stippled line). The ANCOVA results showed that differences between two datasets were significant for both the slope (homogeneity of regressions, $p < 0.0001$) and the intercept ($p < 0.0001$). This indicates that the TEX_{86}^H values in the Mediterranean Sea must be influenced by additional factors rather than only annual mean SST.

To examine the distribution of isoGDGTs, principal components analysis (PCA) on the fractional abundances
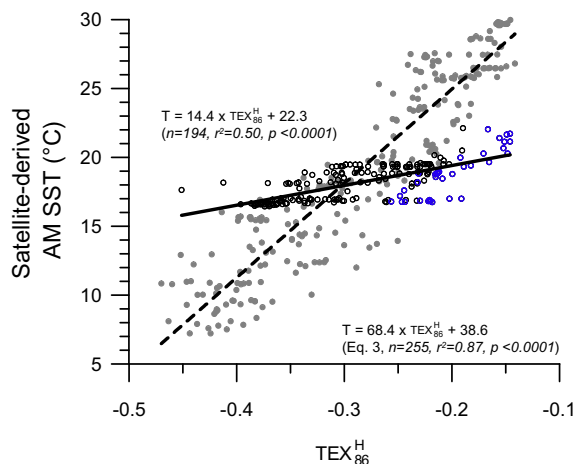
Fig. 4. Cross plots of satellite-derived SSTs with TEX_{86}^H values of the Mediterranean core-top dataset (black line, black circles) and with those of the global core-top dataset (Eq. (3), stippled line, grey filled circles) of Kim et al. (2010a). The Mediterranean data from >1000 m water depth are indicated as blue circles. (For interpretation of the references to colour in this figure legend, the reader is referred to the web version of this article.)

of all isoGDGTs was performed. The first two components explained a cumulative 88% of the variance (Fig. 5A). On the first principal component (PC1, explaining 72% of the variance) the loading of GDGT-0 was opposite to that of all other isoGDGTs. Crenarchaeol positively loaded on the second principal component (PC2, explaining 16% of the variance), against all other isoGDGTs. GDGT-1, -2, -3, and the crenarchaeol regio-isomer were clustered together in the same quadrant in the PCA biplot. Interestingly, these are the components used for the TEX_{86}^H proxy.

To examine which environmental factors controlled the variability in isoGDGT distributions, we performed redundancy analysis (RDA) using all six isoGDGTs (data not shown). The RDA results showed that among the environmental variables annual mean SST (AM SST), the BIT index (a proxy for continental-derived organic matter input) and water depth explained most of the variability in isoGDGT distributions (Table 1). Therefore, we limited the RDA to only these three environmental variables (Fig. 5B). The explanatory (i.e., environmental) variables explained 74% of the variation in the response (i.e., fractional abundance of isoGDGTs) variables. Similar to the PCA results, GDGT-0 was positively loaded on the first axis of RDA (RDA1, explaining 65% of the variance), opposite to all other isoGDGTs. The second axis of RDA (RDA2) explained 9% of the variance. GDGT-1 and crenarchaeol were positively loaded on the RDA2, while GDGT-2, -3, and crenarchaeol regio-isomer were negatively loaded. The RDA results indicated that the isoGDGTs were mostly influenced by three environmental factors, i.e., annual mean SST (49%), continental-derived organic matter input (15%), and water depth (9%).

To examine the environmental factors controlling the TEX_{86}^H proxy, we also performed RDA using only the four isoGDGTs used for the TEX_{86}^H calculation (Fig. 5C).

○ sediments from <200 m water depth
○ sediments from >200 m water depth
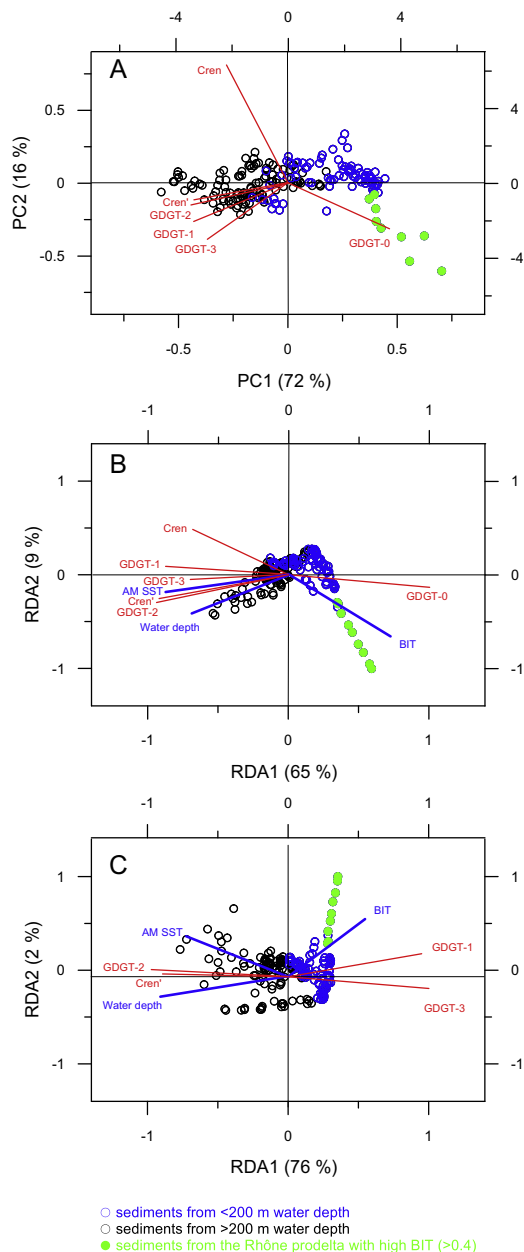● sediments from the Rhône prodelta with high BIT (>0.4)

Fig. 5. (A) PCA biplot of the isoGDGT distributions. The first principal component (PC1) explained 72% of the variation and the second principal component (PC2) 16% of the variation. (B) Triplot obtained by the RDA using six isoGDGTs. 65% of the variation was explained by the first axis (RDA1) and 9% of the variation by the second axis (RDA2). (C) RDA triplot based on only four isoGDGTs used for TEX_{86}^H. The RDA1 explained 76% of the variation and the RDA2 2% of the variation. AM SST, Cren, and Cren′ indicate annual mean SST, crenarchaeol, and crenarchaeol region-isomer, respectively. The BIT index was used as an indicator of the continental-derived organic matter input. Red and blue lines indicate the loading of response (isoGDGTs) and explanatory (environmental) variables, respectively. Blue open circles indicate the scores of the samples from <200 m water depth, black open circles from >200 m water depth, and green filled circles from the Rhône prodelta with high BIT values (>0.4). (For interpretation of the references to colour in this figure legend, the reader is referred to the web version of this article.)

Table 1

(A) Numerical output of the RDA applied for all six isoGDGTs. The sum of all canonical eigenvalues is 0.8 and the total variance is 1. λ (eigenvalue) is the standard deviation of the scores. λ as % of sum of all canonical eigenvalues is obtained by multiplying 0.8 (the sum of all canonical eigenvalues) with the variation explained by the first two axes. (B) The results of the forward selection. % of variance indicates the total sum of eigenvalues after including new explanatory variables. T and PP indicate temperature and primary productivity. Significance level: $p < 0.05$.

RDA axis	λ	λ as % of total inertia	λ as cumulative% of total inertia	λ as % of sum of all canonical eigenvalues
A				
1	0.65	65	65	82.1
2	0.09	9	74	93.9
B				
Order	Explanatory variable	% of variance	F-Statistic	p-Value
1	**AM SST**	**49**	**186.9**	**0.005**
2	**BIT**	**15**	**77.9**	**0.005**
3	**Water depth**	**9**	**60.9**	**0.005**
4	Fall PP	2	17.8	0.005
5	Spring PP	2	12.8	0.005
6	Summer T	1	7.1	0.005
7	Winter PP	1	7.4	0.005
8	Winter T	1	5.9	0.005
9	Spring T	0	2.5	0.060
10	Summer PP	0	1.2	0.305
11	Fall T	0	0.7	0.590

GDGT-1 and GDGT-3 were positively loaded on the RDA1, as opposed to GDGT-2 and crenarchaeol regio-isomer, explaining 76% of the variance. RDA2 explained only 2% of the variance. Considering only four isoGDGTs, water depth explained 63% of the variance, while annual mean SST and continental-derived organic matter input accounted for another 14% and 2% of the variance in isoGDGT distributions, respectively (Table 2). The differences

Table 2

As Table 1 but using only four isoGDGTs: (A) numerical output of the RDA and (B) the results of the forward selection. Significance level: $p < 0.05$.

RDA axis	λ	λ as% of total inertia	λ as cumulative% of total inertia	λ as% of sum of all canonical eigenvalues
A				
1	0.76	76	76	97.4
2	0.02	2	78	99.6
Order	Explanatory variable	% of variance	F-Statistic	p-Value
B				
1	**Water depth**	**63**	**328.6**	**0.005**
2	**AM SST**	**14**	**112.6**	**0.005**
3	**BIT**	**2**	**13.9**	**0.005**

between the two RDA analyses are likely due to the overpowering effect of GDGT-0 and crenarchaeol, which are the two dominant isoGDGTs. GDGT-0 may also have multiple archaeal sources and including this isoGDGT will make the RDA analysis less sensitive to factors which influence the subtle changes in distribution of the minor isoGDGTs.

4. DISCUSSION

Our results show that TEX_{86}^H does not correlate well with annual mean SST in the Mediterranean Sea. We discuss potential environmental factors affecting the isoGDGT distributions and thus the TEX_{86}^H paleothermometer in the following sections.

4.1. Influence of continental isoGDGTs

The surface sediments from the shallow Rhône prodelta area (<100 m water depth) have positive scores on the RDA1, along with the BIT index (green filled data points; Fig. 5B and C). The RDA results thus suggest that continental-derived, i.e., soil- and/or river-derived (cf. Hopmans et al., 2004; Zell et al., 2013a,b; De Jonge et al., 2014) organic matter input, as reflected in the BIT index (e.g., Hopmans et al., 2004), influences the distribution of isoGDGTs (Tables 1 and 2; Fig. 5). The BIT index values are, in general, substantially higher in surface sediments of the continental shelf (<200 m water depth) than in sediments of the continental slope and rise (>200 m water depth) (Fig. 6A) and are especially elevated in the prodeltas of the Rhône River and Po River (Fig. 7A and B, respectively). SPM collected along the Rhône River (SE France) in May 2010 have a high average BIT value of 0.89, and SPM sampled at the Rhône River mouth influenced by the seawater have an average BIT value of 0.65 (Kim et al., 2014). Soils often contain isoGDGTs derived from diverse soil archaea such as Euryarchaeota and Thaumarchaeota (e.g., Leininger et al. 2006; Weijers et al., 2006; Tourna et al., 2011; Sinninghe Damsté et al., 2012). Taken together with previous studies in this region (e.g., Kim et al., 2010b; Tesi et al., 2011), the elevated BIT values in the coastal zones of the Gulf of Lions and the Adriatic Sea indicate that the contribution of continental-derived isoGDGTs is probably higher in the inner shelf areas than the outer shelf areas (Fig. 7A and B). Hence, TEX_{86}^H values of coastal marine sediments that receive continental-derived organic matter, especially near river outflows, may be affected by continental isoGDGTs in the Mediterranean Sea.

Surprisingly, the reconstructed TEX_{86}^H temperatures off the Rhône and Po River mouths, where BIT values are highest (>0.4; Fig. 7A and B), are still well within the error range of the TEX_{86}^H proxy (Fig. 7C and D), with the average ΔT (the difference between TEX_{86}^H-derived temperatures using Eq. (3) and satellite-derive SSTs) value of -0.5 ± 1.3 °C ($n = 10$). This is somewhat unexpected given that previous studies in the equatorial Atlantic and the North Sea showed that the high inputs of continental isoGDGTs (i.e., high BIT values) were associated with a
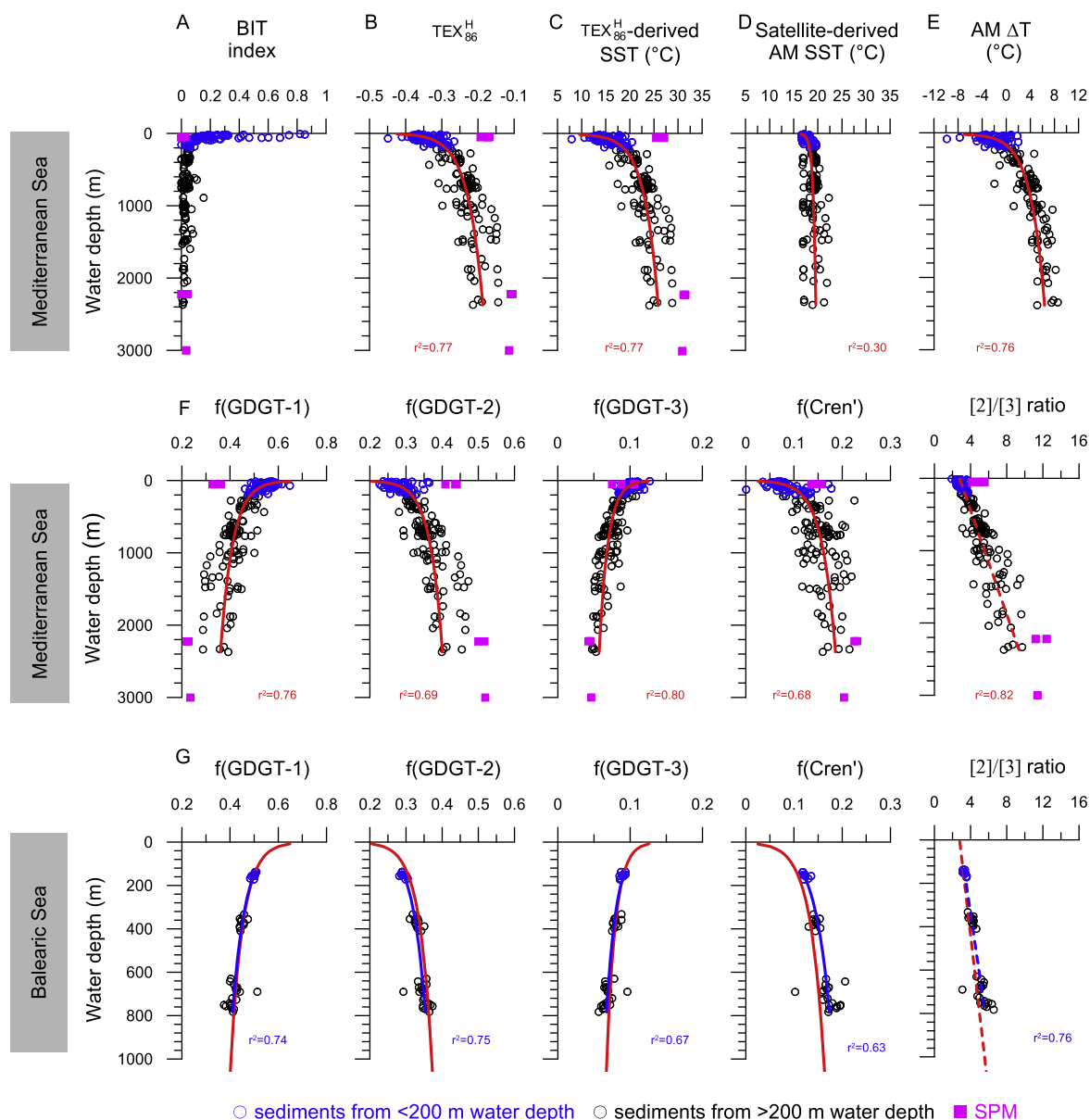
Fig. 6. Vertical water depth profiles of (A) the BIT index, (B) TEX_{86}^H, (C) TEX_{86}^H-derived temperatures using Eq. (3), (D) satellite-derived annual mean SSTs, (E) ΔT between TEX_{86}^H-derived SSTs using Eq. (3) and satellite-derived annual mean SSTs, (F) fractional abundances of isoGDGTs (based on the four isoGDGTs that are used in TEX_{86}^H) and the [2]/[3] ratio (Taylor et al., 2013) for the entire Mediterranean dataset, and (G) fractional abundances of isoGDGTs and the [2]/[3] ratio for the dataset of the Balearic Sea. Blue open circles indicate the data from the shallow shelf areas (<200 m water depth) and black open circles from deeper water depth (>200 m water depth). Logarithmic (solid) or linear (dashed) regression lines are plotted for the Mediterranean Sea (red line) and the Balearic Sea (blue line) datasets. Determination coefficient (r^2) values are given. Filled purple squares indicate the SPM data. The SPM data were not used for the regression of the data. (For interpretation of the references to colour in this figure legend, the reader is referred to the web version of this article.)

substantial bias in TEX_{86}^H-derived SSTs (Herfort et al., 2006; Weijers et al., 2006). Our study indicates that influence of continental-derived isoGDGTs on the TEX_{86}^H proxy may depend on the end-member GDGT distribution of the river drainage basin, i.e., if the TEX_{86}^H distributions of soils or river SPM in the drainage basin are similar to those in the coastal marine waters the bias might be relatively minor (cf. Schouten et al., 2013). Interestingly, much larger

temperature deviations with negative ΔT values (i.e., TEX_{86}^H-derived SSTs < satellite-derived SSTs) are observed on the continental shelves (Fig. 7C and D), where BIT values (<0.05) are much below the cut off value (0.3) proposed earlier (Weijers et al., 2006). Hence, it seems that the continental-derived isoGDGT input is not the main cause for the cold bias of the TEX_{86}^H estimates observed along the coasts of the Gulf of Lions and the Adriatic Sea.

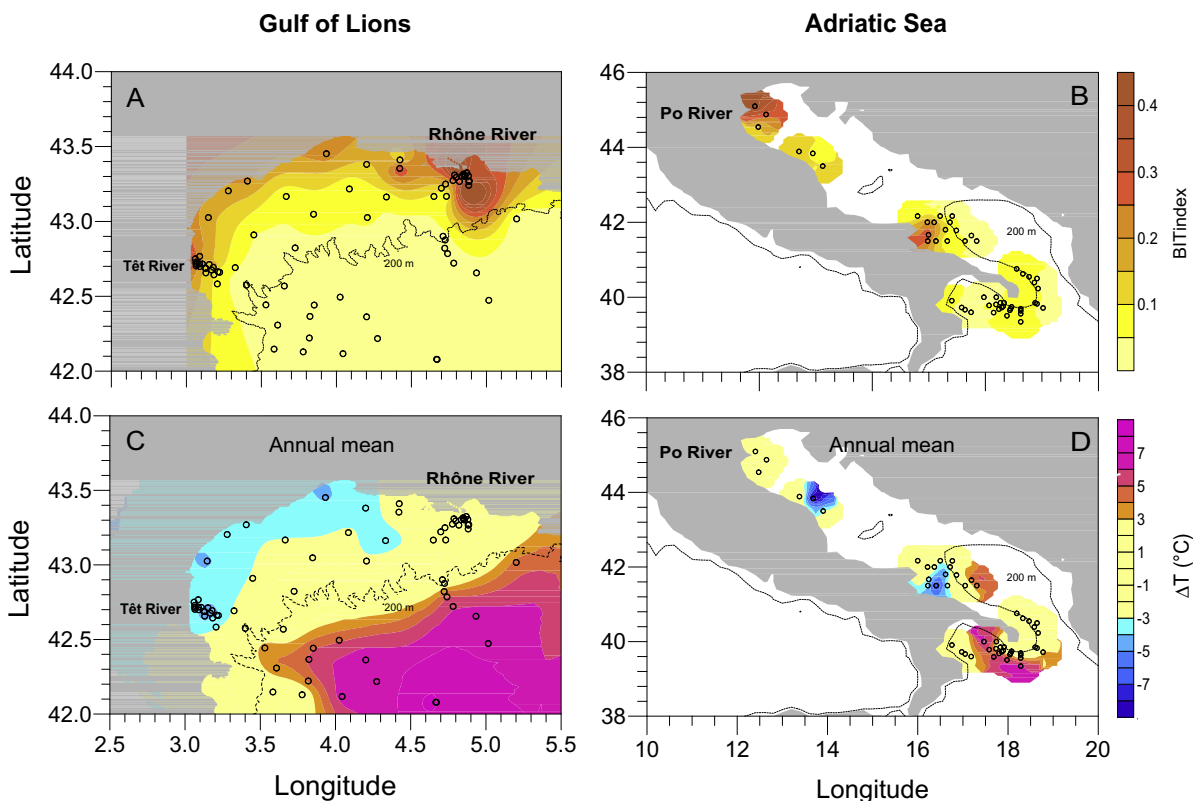Fig. 7. Spatial distribution patterns of (A and B) the BIT index and (C and D) the temperature differences (ΔT) between TEX_{86}^H-derived temperatures using Eq. (3) and satellite-derived annual mean SSTs for the Gulf of Lions and the Adriatic Sea. The spatial distribution pattern was based on the variogram analysis and ordinary kriging, interpolating the data to a 1° × 1° grid with 0.5° × 0.5° searching radius. (For interpretation of the references to colour in this figure legend, the reader is referred to the web version of this article.)

4.2. Seasonal influences

In previous studies, the predominant production and export of Thaumarchaeota during warm (summer/autumn) seasons have been invoked to explain TEX_{86}^H results from surface sediments and paleorecords (Menzel et al., 2006; Castañeda et al., 2010; Leider et al., 2010; Huguet et al., 2011; Grauel et al., 2013; Nieto-Moreno et al., 2013) in the Mediterranean Sea. For spring and winter, temperature differences (ΔT) between TEX_{86}^H – and satellite-derived SSTs in our Mediterranean core-top dataset are larger (up to 12 °C) than those for the annual mean (Fig. 3B and E). However, for summer and autumn, ΔT is reduced (up to 6 °C), suggesting that TEX_{86}^H-derived SSTs indeed agree better with warmer summer/autumn SSTs (Fig. 3C and D). Hence, our results seemingly support previous studies, which suggested that TEX_{86}^H-derived SSTs were skewed towards warm (summer/autumn) seasons in most of the Mediterranean Sea (Menzel et al., 2006; Leider et al., 2010; Castañeda et al., 2010; Huguet et al., 2011; Grauel et al., 2013; Nieto-Moreno et al., 2013). However, it should be noted that for some areas (Fig. 3C and D), TEX_{86}^H still overestimates seasonal SSTs for the warm (summer/ autumn) seasons by up to 6 °C. Based on the RDA results, the satellite-derived annual mean SST is overall the most significant environmental factor rather than seasonal SSTs

(Table 1). Furthermore, a molecular ecology study conducted in the NW Mediterranean Sea (Blanes Bay Microbial Observatory) found that the abundance of Group I Crenarchaeota (i.e., Thaumarchaeota) was highest during winter when water was nutrient-enriched (Galand et al., 2010). Hence, it appears that seasonal differences between the timing of the Thaumarchaeota blooms or exports cannot fully explain a warm bias of the TEX_{86}^H proxy at deep-water sites in the Mediterranean Sea.

4.3. Influence of water depth

Surprisingly, the RDA results show that the distributions in surface sediments of isoGDGTs used in TEX_{86}^H is influenced by water depth. Indeed, the TEX_{86}^H ($r^2 = 0.77$, Fig. 6B) and its derived SSTs ($r^2 = 0.77$, Fig. 6C) show strong positive correlations with water depth, while satellite-derived annual mean SST is only weakly correlated with water depth ($r^2 = 0.30$, Fig. 6D). As a result, the temperature difference (ΔT) shows a substantial increase with water depth ($r^2 = 0.76$, Fig. 6E). This is independent of calibration models, as a similarly strong water depth trend in SST estimates based on the Bayesian regression model BAYSPAR (Tierney and Tingley, 2014) is also apparent (data not shown). Examination of the RDA results shows that surface sediments from the meso-bathypelagic zone

(>200 m water depth) score negatively on RDA1 along with water depth and the fractional abundances of GDGT-2 and crenarchaeol regio-isomer, while GDGT-1 and GDGT-3 score positively on RDA1 (Fig. 5C). Indeed, there is a strong trend when the fractional abundances of the iso-GDGTs used in TEX_{86}^H are plotted versus water depth; decreasing fractional abundances of GDGT-1 and GDGT-3 and increasing fractional abundances of GDGT-2 and crenarchaeol regio-isomer with water depth (Fig. 6F). This water depth dependence is also illustrated by examining a subset of surface sediments from the Balearic Sea, located within a small geographical area (Fig. 2A) with similar annual mean SSTs (on average 19.4 ± 0.1 °C) and presumably similar other environmental factors such as nutrient concentrations. In this region, strong correlations of the fractional abundances of iso-GDGTs with water depth are also observed (Fig. 6G).

A recent study by Taylor et al. (2013) suggested that Thaumarchaeota thriving in deeper waters (>1000 m water depth) might have a different distribution of isoGDGTs, with a higher abundance of GDGT-2 relative to GDGT-3 and consequently a high (>5) GDGT-2/GDGT-3 ratio (i.e., [2]/[3] ratio). They argued that this would explain the positive correlation of the [2]/[3] ratio with water depth seen in the Kim et al. (2010a) dataset of surface sediments. In agreement with this, the [2]/[3] ratio in surface sediments strongly increases with water depth in the Mediterranean Sea as well as in the Balearic Sea (Fig. 6F and G). Hence, our results potentially support the idea that deep-water dwelling Thaumarchaeota may have different distributions of isoGDGTs in comparison to those of shallow ones. In addition to the fractional abundance of GDGT-2, our data show that the fractional abundance of the crenarchaeol regio-isomer equally strongly increases with water depth, which was not observed by Taylor et al. (2013) in the global core top dataset of Kim et al. (2010a). The higher fractional abundance of GDGT-2 and crenarchaeol regio-isomer and the lower fractional abundance of GDGT-1 and GDGT-3, possibly produced by Thaumarchaeota thriving below the mixed-layer, explain the higher TEX_{86}^H values in surface sediments from areas with a deeper water-column (Fig. 6B) and, consequently, the higher ∆T.

Molecular biological studies have shown that thaumarchaeotal sequences from the meso-bathypelagic (>200 m water depth) waters are phylogenetically different from those retrieved from the epipelagic (0–200 m water depth) waters (e.g., Francis et al., 2005; Hu et al., 2011a,b; Yakimov et al., 2011; Sintes et al., 2012; Schouten et al., 2012) and thus may have a different isoGDGT distribution. Villanueva et al. (2014) showed essential amino acid differences in geranylgeranylglyceryl phosphate (GGGP) synthase, a key gene of the GDGT biosynthetic pathway, between 'shallow water' and 'deep water' Thaumarchaeota residing in the ocean. They attributed observed differences in isoGDGT distributions from subsurface to deep waters to the differences in archaeal population of shallow and deep waters. Differences in isoGDGT distributions have been previously documented for different cultivated species of Thaumarchaeota, e.g., Group 1.1b Thaumarchaeota produce the crenarchaeol regio-isomer in a higher

fractional abundance than Group 1.1a Thaumarchaeota (Sinninghe Damsté et al., 2012).

To test the hypothesis of different archaeal populations in different water masses, we analyzed SPM collected from shallow (50 m water depth) and deep (2000–3000 m water depth) water masses of the Mediterranean Sea. Crenarchaeol ($46 \pm 1\%$ of total isoGDGTs) is the most abundant iso-GDGT in the shallow-water SPM, followed by GDGT-0 ($28 \pm 2\%$). The most abundant isoGDGT in the deep-water SPM is also crenarchaeol ($47 \pm 2\%$), but GDGT-0 is less abundant ($18 \pm 1\%$). Interestingly, when we focus on the fractional abundances of isoGDGTs that are used for the TEX_{86}^H paleothermometer, GDGT-2 ($51 \pm 1\%$) and the crenarchaeol regio-isomer ($22 \pm 1\%$) are much more dominant in the deep-water SPM than in the shallow-water SPM, while the fractional abundances of GDGT-1 and GDGT-3 show an opposite trend (Fig. 8A and B). This is in line with the idea that the isoGDGT distribution in deeper waters might be different from that in surface waters
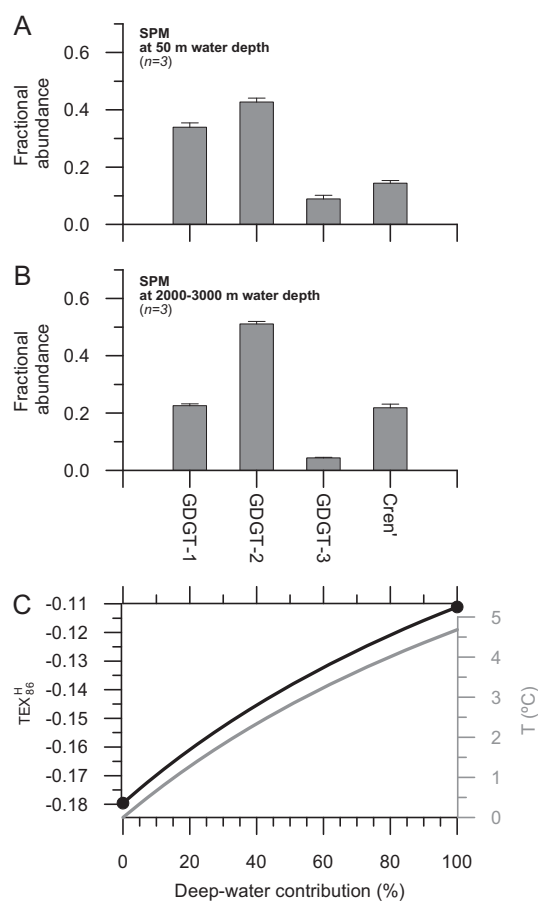

Fig. 8. Hypothetical binary mixing model showing the effect of the contribution of deep-water dwelling Thaumarchaeota on sedimentary isoGDGTs (C) using two end members representing the average distribution of isoGDGTs used for the TEX_{86}^H (A) of the surface mixed layer and (B) of the deep waters. Different mixing ratios result in different values for the TEX_{86}^H proxy (black line) with the accompanying ∆T (grey line). End-member TEX_{86}^H values are indicated with closed circles.

due to presence of a different thaumarchaeotal community. TEX_{86}^H values of the shallow-water SPM are on average -0.18 ± 0.01 while those of the deep-water SPM are higher with the average value of -0.11 ± 0.004. Accordingly, the resulting TEX_{86}^H-derived temperature is higher for the deep-water SPM (with an average value of $31.0 \pm 0.2 \,°C$) than for the shallow-water SPM (on average $26.3 \pm 0.7 \,°C$) (end member values in Fig. 6C). These TEX_{86}^H-derived temperatures differ from the temperature profile in the water, which drops from $\sim 25 \,°C$ at 50 m water depth to $\sim 14 \,°C$ at water depths >2000 m.

The trend observed in the SPM is identical to the observed trend in the isoGDGT distribution in surface sediments with increasing water depth (i.e., increased fractional abundance of GDGT-2 and the crenarchaeol regio-isomer and increased TEX_{86}^H values in surface sediments deposited in deep water; Fig. 6). Our SPM data, therefore, support the idea that deep-water dwelling Thaumarchaeota produce isoGDGTs with a higher fractional abundance of GDGT-2 and the crenarchaeol regio-isomer and a lower fractional abundance of GDGT-1 and GDGT-3. With increasing water depth, this deep-water population of Thaumarchaeota may increasingly contribute to the pool of sedimentary isoGDGTs, thereby influencing the TEX_{86}^H proxy. To further constrain this, we performed a simple two end-member mixing model, by using the distribution of isoGDGTs of the shallow-water SPM as the surface end-member and that of the deep-water SPM as the deep-water end-member. The results show that the TEX_{86}^H-derived SST will substantially deviate from the surface end-member value of $26.3 \,°C$ with an increasing contribution of isoGDGTs produced in deeper waters (Fig. 8C).

4.4. Distribution of isoGDGTs in deep restricted basins

Our results suggest that there are two major isoGDGT inputs to surface sediments of the Mediterranean Sea: one derived from shallow-water and the other from deep-water dwelling thaumarchaeotal populations. This implies that it will be difficult to predict annual mean SSTs using Eq. (3) (global core-top calibration) of Kim et al. (2010a), especially for deep basins in the Mediterranean Sea. Therefore, we investigated which factors predominantly control the distribution of isoGDGTs in the Mediterranean deep restricted basins. We observe that TEX_{86}^H values in surface sediments from > 1000 m water depth do not correlate with water depth ($r^2 = 0.03$, Fig. 9A). Subsequently, we compared TEX_{86}^H values with temperature at 1000 m water depth, assuming that isoGDGTs purely originated from deep waters, but again a weak correlation is observed ($r^2 = 0.30$; Fig. 9B). Instead, we find that TEX_{86}^H values are strongly associated with satellite-derived annual mean SST ($r^2 = 0.74$; Fig. 9C). Hence, it seems that although sediments deposited in deep waters (>1000 m water depth) receive a substantial contribution of isoGDGTs from a deep-water thaumarchaeotal population, they still reflect a signal which is related to surface water conditions.

It has been observed previously that TEX_{86} in the northern Red Sea, another regional restricted basin, had a strongly different correlation with annual mean SST (Trommer et al., 2009). Notably, most of sediments investigated were taken from deep waters (600–1600 m water depth), suggesting a similar phenomenon as observed for the Mediterranean Sea. Therefore, we have established a composite dataset of deep-water (>1000 m water depth) surface sediments from deep restricted basins in this interconnected region, i.e., the Mediterranean Sea and the northern Red Sea (data from Trommer et al., 2009). As observed for the Mediterranean Sea dataset, the composite dataset shows no significant relationship between TEX_{86}^H and water depth ($r^2 = 0.04$). However, the composite dataset also shows a strong correlation between TEX_{86}^H and satellite-derived annual mean SST (Fig. 9C) which can be described by the following equation:

$$T = 56.3 \times TEX_{86}^H + 30.2 \quad (r^2 = 0.94, \ n = 45,$$
$$p < 0.001, 0 \text{ m water depth}) \tag{4}$$

The residual standard error in temperature estimates using this calibration model is only $1 \,°C$. This suggests that in the northern Red Sea, there may be controlling mechanisms on the distribution of isoGDGTs in surface sediments common to those operating in the Mediterranean Sea; i.e., a deep-water population of Thaumarchaeota affecting the sedimentary isoGDGT signal, but not in such a way that the influence of surface water temperatures is eliminated. Interestingly, this deep restricted basin dataset forms a distinctive correlation line in comparison to that of the global core-top dataset (Kim et al., 2010a) (Fig. 9D) with significant differences between both datasets for both the intercept ($df = 1$, $F = 230$, $p = <0.001$) and the slope ($df = 1$, $F = 4.06$, $p = 0.04$). We also observe this difference if we consider only the TEX_{86}^H data from surface sediments deposited at >1000 m water depth in the global core-top dataset (yellow filled circles, Fig. 9D).

When we follow the approach applied by Kim et al. (2008) and correlate TEX_{86}^H values of surface sediments from >1000 m water depth with depth-integrated annual mean temperatures for 0 to 200 m water depth an equally strong relation is found:

$$T = 57.6 \times TEX_{86}^H + 27.1 \quad (r^2 = 0.90, \ n = 44,$$
$$p < 0.0001, 0–200 \text{ m water depth}) \tag{5}$$

This relationship (Eq. (5); Fig. 9E) also significantly differs from that of the global core-top dataset (Fig. 9F) for the intercept ($df = 1$, $F = 116.5$, $p = <0.001$), similar to the SST calibration (Eq. (4); Fig. 9D), but not for the slope ($df = 1$, $F = 0.32$, $p = 0.57$).

The reason for this difference between the global core-top dataset and the deep-water restricted basin dataset remains to be fully understood. It is noteworthy that these deep restricted basins are all characterized by higher (i.e., $\sim 13 \,°C$ for the Mediterranean Sea and $\sim 22 \,°C$ for the Red Sea) bottom water temperatures than the open ocean (i.e., $4–6 \,°C$) (Locarnini et al., 2013). Warmer deep waters in these restricted basins imply that more organic matter is mineralized in the deeper part of the water column compared to open oceans. This increased break-down of organic matter in bottom waters will result in a higher ammonium generation rate. Since Thaumarchaeota are
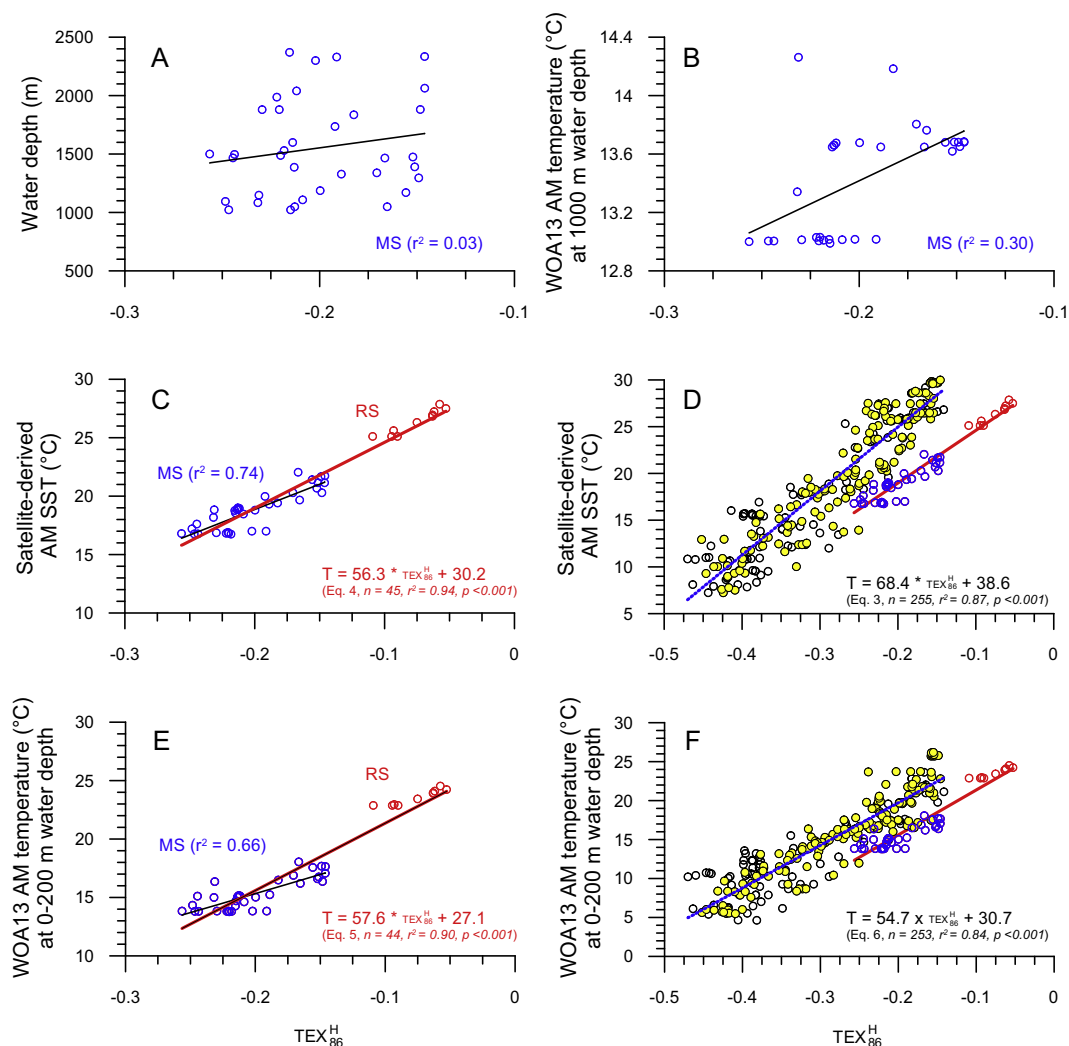
Fig. 9. Cross plots of TEX_{86}^{H} data for surface sediments from > 1000 m water depth in the Mediterranean Sea (blue circles) and the Red Sea (red circles) (A) with water depth, (B) with annual mean temperature at 1000 m water depth from the World Ocean Atlas 13 (WOA13) dataset (Locarnini et al., 2013), (C and D) with satellite-derived annual mean SSTs, and (E-F) with depth-integrated annual mean WOA13 temperature for 0–200 m water depth. The data are compared with the global core-top dataset of Kim et al. (2010a) (D) based on satellite-derived annual mean SSTs (Eq. (3)) and (F) based on depth-integrated annual mean temperatures for 0–200 m water depth (Eq. (6)). The global core-top data from >1000 m water depth are indicated as yellow filled circles. RS and MS indicate the Red Sea and the Mediterranean Sea, respectively. (For interpretation of the references to colour in this figure legend, the reader is referred to the web version of this article.)

nitrifiers (e.g., Könneke et al., 2005; Wuchter et al., 2006; Yakimov et al., 2011) this may sustain a relatively abundant population of deep water dwelling Thaumarchaeota that apparently have a different GDGT composition in this type of deep restricted basins. This may result in a stronger contribution of deep water Thaumarchaeota in sediments compared to open ocean settings where a trend with water depth is not observed in TEX_{86} values (Tierney and Tingley, 2014). This deep water contribution alters the TEX_{86}^{H} values but in such a way that apparently the temperature signal from the upper water column (i.e., epipelagic zone) remains apparent. However, because of the deep water contribution, the relationship between TEX_{86}^{H} values and temperatures of the upper water column is now different compared to that of open ocean settings.

4.5. Testing the deep-water TEX_{86}^{H}-SST relationship at >1000 m water depth sites

Here we examine if the new empirical relationship based on sedimentary isoGDGT data from >1000 m water depth in the marginal, landlocked seas (Eq. (4)) would better predict annual mean SST changes in the deep restricted basins at water depth >1000 m than the global core-top calibration (Eq. (3); Kim et al., 2010a). We converted TEX_{86}^{H} values to SSTs using both Eq. (3) (global core-top calibration) and Eq. (4) ('deep-water calibration') for two sediment cores from the Alboran Sea in the western Mediterranean Sea (Fig. 2A): core 434G (1108 m water depth) and core 293G (1840 m water depth) and compared them with previously published $U_{37}^{K'}$-derived SSTs (Rodrigo-Gámiz et al.,

2014). As an alternative approach to the global core-top calibration and the regional deep water calibration, we estimated SSTs using the BAYSPAR calibration model, applying the "standard prediction" mode, which assumes that the oceanographic conditions are sufficiently similar to present day, and using the default settings (Tierney and Tingley, 2014).

Cores 434G and 293G from the western and eastern Alboran Sea (Rodrigo-Gámiz et al., 2014) cover the last 14 and 20 kyr, respectively (Fig. 10A and B). For core 293G, $U_{37}^{K'}$-derived SSTs vary between 10 and 20 °C, with an SST increase of ca. 7 °C from the end of the Last Glacial Maximum (LGM) to the Early Holocene (Rodrigo-Gámiz et al., 2014). For core 434G, $U_{37}^{K'}$-derived SSTs range from 14 to 22 °C, following those observed for core 293G, but being ca. 2 °C higher during most of the Holocene (Rodrigo-Gámiz et al., 2014). The higher $U_{37}^{K'}$-derived SSTs in the western Alboran Sea were interpreted as resulting from a southeastward migration of cold waters to the eastern Alboran Sea during late autumn and spring and a resulting divergence in the haptophyte blooming seasons between the western and eastern Alboran Sea (Rodrigo-Gámiz et al., 2014). TEX_{86}^{H}-derived SSTs using the global core top calibration (Eq. (3); Kim et al., 2010a) are much

higher (red curve) for both cores, with a range of 11–26 °C for core 293G and 17–26 °C for core 434G. In contrast, when TEX_{86}^{H} values are translated into SSTs using the empirical 'deep-water calibration' (Eq. (4); blue curve), TEX_{86}^{H}-derived SSTs are much closer to $U_{37}^{K'}$-derived ones, with a range of 9–20 °C for core 293G and 13–20 °C for core 434G. Similarly, SST estimates using the BAYSPAR calibration vary between 7 and 22 °C for core 293G and between 12 and 22 °C for core 434G. All three TEX_{86}^{H}-derived records are quite similar compared to each other, with the same range of temperatures as the $U_{37}^{K'}$-derived SSTs from the eastern Alboran Sea during the Holocene. However, the TEX_{86}^{H}-derived temperature difference between the LGM and the Early Holocene is somewhat larger (9 °C for the deep water calibration, and 11 °C for the BAYSPAR) than that derived from $U_{37}^{K'}$ (7 °C). This is due to lower TEX_{86}^{H}-derived SSTs during the LGM than the $U_{37}^{K'}$-derived SSTs. The BIT values (green curve) are well below the cut-off value of 0.3 (Weijers et al., 2006). Therefore, an impact of continental-derived organic matter input on the TEX_{86}^{H} values is likely negligible. Together, this study shows that the regional relationship between TEX_{86}^{H} and SST for deep-water restricted basins as well as the BAYSPAR calibration, which effectively allows for regional variations in calibrations, may be applicable over glacial to interglacial time scales. It also supports our finding that seasonality may not be a primary cause for a warm bias of the TEX_{86}^{H} proxy in the Mediterranean Sea. Further research is required before this relationship can be confidently applied as a calibration to estimate temperatures in the Mediterranean Sea and the northern Red Sea.

5. CONCLUSIONS

We investigated isoGDGT distributions of core-top sediments and SPM from the Mediterranean Sea and discussed potential environmental factors influencing the TEX_{86}^{H} paleothermometer. We observe that TEX_{86}^{H}-derived SSTs were much cooler along the coast than the satellite-derived annual mean SSTs, while warmer TEX_{86}^{H}-derived SSTs prevailed at deep-water sites. Our RDA results showed that, when considering only the four isoGDGTs that are used for the TEX_{86}^{H} proxy, water depth is the most significant parameter. In fact, one of the most striking features in our dataset is a strong positive relationship between water depth and TEX_{86}^{H} due to elevated fractional abundances of GDGT-2 and crenarchaeol regio-isomer and lower abundances of GDGT-1 and GDGT-3 at deep-water sites. Most likely, Thaumarchaeota thriving in deep-water masses produce isoGDGTs in different distributions in comparison to those of surface-dwelling Thaumarchaeota. Intriguingly, the TEX_{86}^{H} data from the deep-water (bathypelagic) part (>1000 m water depth) are not correlated anymore with water depth but instead are strongly correlated with annual mean SSTs. The composite deep-water TEX_{86}^{H} dataset composed of the Mediterranean Sea and the northern Red Sea surface sediments at >1000 m shows a correlation with SST that is clearly distinct from the global core-top dataset. By applying this deep-water relationship, the TEX_{86}^{H} SST estimates for two sediment cores from the Alboran Sea in the
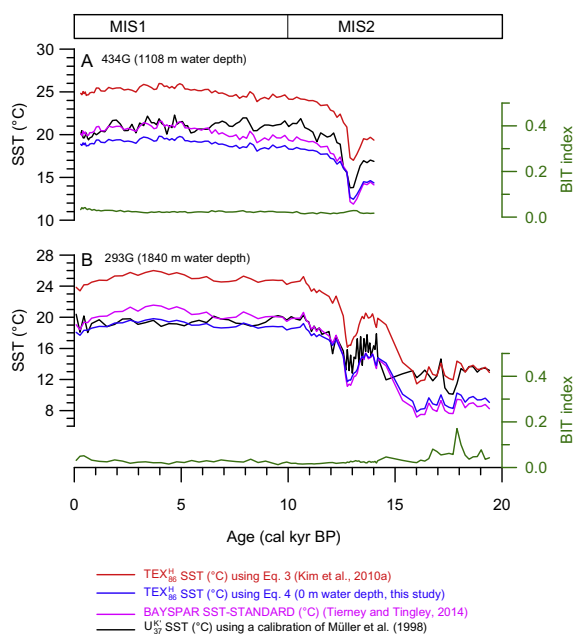

Fig. 10. Application of TEX_{86}^{H} and $U_{37}^{K'}$ proxies and their calibrations to two sediment cores from the western Mediterranean Sea. Three TEX_{86}^{H} records are shown based on the global core-top calibration (red curve), the Mediterranean deep water calibration (blue curve), and the BAYSPAR standard prediction model (purple curve). The $U_{37}^{K'}$ values were converted into temperature values (black curves) applying a global core-top calibration $((T = U_{37}^{K'} - 0.044)/0.033)$ of Müller et al. (1998): (A) core 434G (36°12.313 N, 4°18.735 W; 1108 m water depth; Rodrigo-Gámiz et al., 2014) and (B) core 293G (36°10.414 N, 2°45.280 W; 1840 m water depth; Rodrigo-Gámiz et al., 2014). The BIT index was shown as green curves. MIS indicates marine isotope stage. (For interpretation of the references to colour in this figure legend, the reader is referred to the web version of this article.)

western Mediterranean Sea are much closer to $U_{37}^{K'}$-derived SSTs than those using the global core-top calibration. This suggests that a regional calibration based on a deep-water TEX_{86}^H dataset may be applicable for deep restricted basins to reconstruct past ocean water temperatures, although the reason remains unclear. Clearly, more detailed water-column studies covering different seasons, water depths, and oceanographic provinces are essential for better understanding export dynamics of isoGDGTs and thus the extent of the influence of deep-water derived isoGDGTs to sedimentary isoGDGT distributions.

APPENDIX A. SUPPLEMENTARY DATA

Supplementary data associated with this article can be found, in the online version, at http://dx.doi.org/10.1016/j.gca.2014.11.017.

REFERENCES

Behrenfeld M. J. and Falkowski P. G. (1997) A consumer's guide to phytoplankton primary productivity models. *Limnol. Oceanogr.* **42**, 1479–1491.

Bijl P. K., Bendle J. A., Bohaty S. M., Pross J., Schouten S., Tauxe L., Stickley C. E., McKay R. M., Röhl U., Olney M., Sluijs A., Escutia C. and Brinkhuis H.Expedition 318 Scientists (2013) Eocene cooling linked to early flow across the Tasmanian Gateway. *Proc. Natl. Acad. Sci. U.S.A.* **110**, 9645–9650.

Brassell S. C., Eglinton G., Marlowe I. T., Pflaumann U. and Sarnthein M. (1986) Molecular stratigraphy: A new tool for climatic assessment. *Nature* **320**, 129–133.

Brochier-Armanet C., Boussau B., Gribaldo S. and Forterre P. (2008) Mesophilic crenarchaeota: Proposal for a third archaeal phylum, the Thaumarchaeota. *Nat. Rev. Microbiol.* **6**, 245–252.

Casey K. and Cornillon P. (1999) A comparison of satellite and in situ-based sea surface climatologies. *J. Climate* **12**, 1848–1863.

Castañeda I. S., Schefuss E., Patzold J., Sinninghe Damsté J. S., Weldeab S. and Schouten S. (2010) Millennial-scale sea surface temperature changes in the eastern Mediterranean (Nile river delta region) over the last 27,000 years. *Paleoceanography* **25**. http://dx.doi.org/10.1029/2009PA001740.

Dang H., Zhou H., Yang J., Ge H., Jiao N., Luan X., Zhang C. and Klotz M. G. (2013) Thaumarchaeotal signature gene distribution in sediments of the northern South China Sea: An indicator of the metabolic intersection of the marine carbon, nitrogen, and phosphorus cycles? *Appl. Environ. Microbiol.* **79**, 2137–2147.

De Jonge C., Stadnitskaia A., Hopmans E. C., Cherkashov G., Fedotov A. and Sinninghe Damsté J. S. (2014) In-situ produced branched glycerol dialkyl glycerol tetraethers in suspended particulate matter from the Yenisei River, Eastern Siberia. *Geochim. Cosmochim. Acta* **125**, 476–491.

Francis C. A., Roberts K. J., Beman J. M., Santoro A. E. and Oakley B. B. (2005) Ubiquity and diversity of ammonia-oxidizing archaea in water columns and sediments of the ocean. *Proc. Natl. Acad. Sci. U.S.A.* **102**, 14683–14688.

Galand P. E., Gutierrez-Provecho C., Massana R., Gasol J. M. and Casamayor E. O. (2010) Inter-annual recurrence of archaeal assemblages in the coastal NW Mediterranean Sea (Blanes Bay Microbial Observatory). *Limnol. Oceanogr.* **55**, 2117–2125.

Grauel A.-L., Leider A., Goudeau M.-L. S., Müller I. A., Bernasconi S. M., Hinrichs K.-U., de Lange G. J., Zonneveld K. A. F. and Versteegh G. J. M. (2013) What do SST proxies really tell us? A high-resolution multiproxy ($U_{37}^{K'}$, TEX_{86}^H, and foraminifera $\delta^{18}O$) study in the Gulf of Taranto, central Mediterranean Sea. *Quat. Sci. Rev.* **73**, 115–131.

Herfort L., Schouten S., Boon J. P. and Sinninghe Damsté J. S. (2006) Application of the TEX_{86} temperature proxy to the southern North Sea. *Org. Geochem.* **37**, 1715–1726.

Herfort L., Schouten S., Abbas B., Veldhuis M. J. W., Coolen M. J. L., Wuchter C., Boon J. P., Herndl G. J. and Sinninghe Damsté J. S. (2007) Variations in spatial and temporal distribution of Archaea in the North Sea in relation to environmental variables. *FEMS Microbiol. Ecol.* **62**, 242–257.

Herndl G. J., Reinthaler T., Teira E., van Aken H., Veth C., Pernthaler A. and Pernthaler J. (2005) Contribution of Archaea to total prokaryotic production in the deep Atlantic Ocean. *Appl. Environ. Microbiol.* **71**, 2303–2309.

Hopmans E. C., Weijers J. W. H., Schefuß E., Herfort L., Sinninghe Damsté J. S. and Schouten S. (2004) A novel proxy for terrestrial organic matter in sediments based on branched and isoprenoid tetraether lipids. *Earth Planet. Sci. Lett.* **224**, 107–116.

Hu A. Y., Jiao N. Z. and Zhang C. L. (2011a) Community structure and function of planktonic Crenarchaeota: Changes with depth in the South China Sea. *Microb. Ecol.* **62**, 549–563.

Hu A. Y., Jiao N. Z., Zhang R. and Yang Z. (2011b) Niche partitioning of marine group I Crenarchaeota in the euphotic and upper mesopelagic zones of the East China Sea. *Appl. Environ. Microbiol.* **77**, 7469–7478.

Huguet C., Schimmelmann A., Thunell R., Lourens L. J., Sinninghe Damsté J. S. and Schouten S. (2007) A study of the TEX_{86} paleothermometer in the water column and sediments of the Santa Barbara Basin, California. *Paleoceanography* **22**. http://dx.doi.org/10.1029/2006PA001310.

Huguet C., Martrat B., Grimalt J. O., Sinninghe Damsté J. S. and Schouten S. (2011) Coherent millennial-scale patterns in $U_{37}^{K'}$ and TEX_{86}^H temperature records during the penultimate interglacial-to-glacial cycle in the western Mediterranean. *Paleoceanography* **26**. http://dx.doi.org/10.1029/2010PA002048.

Ingalls A. E., Shah S. R., Hansman R. L., Aluwihare L. I., Santos G. M., Druffel E. R. M. and Pearson A. (2006) Quantifying archaeal community autotrophy in the mesopelagic ocean using natural radiocarbon. *Proc. Natl. Acad. Sci. U.S.A.* **103**, 6442–6447.

Jia G., Zhang J., Chen J., Peng P. and Zhang C. L. (2012) Subsurface water temperatures recorded by archaeal tetraether lipids in the South China Sea. *Org. Geochem.* **50**, 68–77.

Karner M. B., DeLong E. F. and Karl D. M. (2001) Archaeal dominance in the mesopelagic zone of the Pacific Ocean. *Nature* **409**, 507–510.

Kim J.-H., Schouten S., Hopmans E. C., Donner B. and Sinninghe Damsté J. S. (2008) Global sediment core-top calibration of the TEX$_{86}$ paleothermometer in the ocean. *Geochim. Cosmochim. Acta* **72**, 1154–1173.

Kim J.-H., van der Meer J., Schouten S., Helmke P., Willmott V., Sangiorgi F., Koç N., Hopmans E. C. and Sinninghe Damsté J. S. (2010a) New indices and calibrations derived from the distribution of crenarchaeal isoprenoid tetraether lipids: Implications for past sea surface temperature reconstructions. *Geochim. Cosmochim. Acta* **74**, 4639–4654.

Kim J.-H., Zarzycka B., Buscail R., Peters F., Bonnin J., Ludwig W., Schouten S. and Sinninghe Damsté J. S. (2010b) Contribution of river-borne soil organic carbon to the Gulf of Lions (NW Mediterranean). *Limnol. Oceanogr.* **55**, 507–518.

Kim J.-H., Romero O. E., Lohmann G., Donner B., Laepple T., Haam E. and Sinninghe Damsté J. S. (2012a) Pronounced subsurface cooling of North Atlantic waters off Northwest Africa during Dansgaard-Oeschger interstadials. *Earth Planet. Sci. Lett.* **339–340**, 95–102.

Kim J.-H., Crosta X., Willmott V., Renssen H., Massé G., Bonnin J., Helmke P., Schouten S. and Sinninghe Damsté J. S. (2012b) Increase in Late Holocene subsurface temperature variability in East Antarctica. *Geophys. Res. Lett.* **39**, L06705. http://dx.doi.org/10.1029/2012GL051157.

Kim J.-H., Buscail R., Fanget A.-S., Eyrolle-Boyer F., Bassetti M.-A., Dorhout D., Baas M., Berné S. and Sinninghe Damsté J. S. (2014) Impact of river channel shifts on tetraether lipids in the Rhône prodelta (NW Mediterranean): Implication for the BIT index as an indicator of palaeoflood events. *Org. Geochem.* http://dx.doi.org/10.1016/j.orggeochem.2014.06.011.

Könneke M., Bernhard A. E., de la Torre J., Walker C. B., Waterbury J. B. and Stahl D. A. (2005) Isolation of an autotrophic ammonia-oxidizing marine archaeon. *Nature* **437**, 543–546.

Kotthoff U., Pross J., Müller U. C., Peyron O., Schmiedl G., Schulz H. and Bordon A. (2008) Climate dynamics in the borderlands of the Aegean Sea during formation of Sapropel S1 deduced from a marine pollen record. *Quat. Sci. Rev.* **27**, 832–845.

Lee K.-E., Kim J.-H., Wilke I., Helmke P. and Schouten S. (2008) U$_{37}^{K'}$, TEX$_{86}$, and planktonic foraminifera in the Benguela Upwelling System: Implications for past sea surface temperature estimates. *Geochem. Geophys. Geosyst.* **9**. http://dx.doi.org/10.1029/2008GC002056.

Leider A., Hinrichs K.-U., Mollenhauer G. and Versteegh G. J. M. (2010) Core-top calibration of the lipidbased U$_{37}^{K'}$ and TEX$_{86}$ temperature proxies on the southern Italian shelf (SW Adriatic Sea, Gulf of Taranto). *Earth Plan. Sci. Lett.* **300**, 112–114.

Leininger S., Urich T., Schloter M., Schwark L., Qi J., Nicol G. W., Prosser J. I., Schuster S. C. and Schleper C. (2006) Archaea predominate among ammonia-oxidizing prokaryotes in soils. *Nature* **442**, 806–809.

Littler K., Robinson S. A., Bown P. R., Nederbragt A. J. and Pancost R. D. (2011) High sea-surface temperatures during the Early Cretaceous Epoch. *Nat. Geosci.* **4**, 169–172.

Liu Z., Pagani M., Zinniker D., DeConto R., Huber M., Brinkhuis H., Shah S. R., Leckie R. M. and Pearson A. (2009) Global cooling during the Eocene–Oligocene climate transition. *Science* **323**, 1187–1190.

Locarnini R. A., Mishonov A. V., Antonov J. I., Boyer T. P., Garcia H. E., Baranova O. K., Zweng M. M., Pave r. C. R.,

Reagan, Johnson D. R., Hamilton M. and Seidov D. (2013) World Ocean Atlas 2013, Volume 1: Temperature. In *NOAA Atlas NESDIS*, vol. 73 (ed. S. Levitus). U.S. Government Printing Office, Washington, D.C., p. 40.

Lopes dos Santos R. A., Prange M., Castañeda I. S., Schefuß E., Mulitza S., Schulz M., Niedermeyer E. M., Sinninghe Damsté J. S. and Schouten S. (2010) Glacial–interglacial variability in Atlantic meridional overturning circulation and thermocline adjustments in the tropical North Atlantic. *Earth Planet. Sci. Lett.* **300**, 407–414.

Marino G., Rohling E. J., Sangiorgi F., Hayes A., Casford J. L., Lotter A. F., Kucera M. and Brinkhuis H. (2009) Early and middle Holocene in the Aegean Sea: Interplay between high and low latitude climate variability. *Quat. Sci. Rev.* **28**, 3246–3262.

Menzel D., Schouten S., Hopmans E. C. and Sinninghe Damsté J. S. (2006) Membrane tetraether lipids of planktonic Crenarchaeota in Pliocene sapropels of the eastern Mediterranean Sea. *Palaeogeogr. Palaeoclimatol. Palaeoecol.* **239**, 1–15.

Müller P. J., Kirst G., Ruhland G., Von Storch I. and Rosell-Melé A. (1998) Calibration of the alkenone paleotemperature index U$_{37}^{K'}$ based on core-tops from the eastern South Atlantic and the global ocean (60°N-60°S). *Geochim. Cosmochim. Acta* **62**, 1757–1772.

Nieto-Moreno V., Martínez-Ruiz F., Willmot V., García-Orellana J., Masqué P. and Sinninghe Damsté J. S. (2013) Climate conditions in the westernmost Mediterranean over the last two millenia: An integrated biomarker approach. *Org. Geochem.* **55**, 1–10.

Pearson A. and Ingalls A. E. (2013) Assessing the use of archaeal lipids as marine environmental proxies. *Ann. Rev. Earth Planet. Sci.* **41**, 15.1–15.26.

Pearson A., McNichol A. P., Benitez-Nelson B. C., Hayes J. M. and Eglinton T. I. (2001) Origins of lipid biomarkers in Santa Monica Basin surface sediment: A case study using compound-specific Δ^{14}C analysis. *Geochim. Cosmochim. Acta* **65**, 3123–3127.

Prahl F. G. and Wakeham S. G. (1987) Calibration of unsaturation patterns in long-chain ketone compositions for paleotemperature assessment. *Nature* **330**, 367–369.

Rodrigo-Gámiz M., Martínez-Ruiz F., Rampen S. W., Schouten S. and Sinninghe Damsté J. S. (2014) Sea surface temperature variations in the western Mediterranean Sea over the last 20 kyr: A dual-organic proxy (U$_{37}^{K'}$ and LDI) approach. *Paleoceanography* **29**, 87–98.

Rohling E. J., Mayewski P. A., Hayes A., Abu-Zied R. H. and Casford J. S. L. (2002) Holocene atmosphere–ocean interactions: Records from Greenland and the Aegean Sea. *Clim. Dyn.* **18**, 587–593.

Schouten S., Hopmans E. C., Pancost R. D. and Sinninghe Damsté J. S. (2000) Widespread occurrence of structurally diverse tetraether membrane lipids: Evidence for the ubiquitous presence of low-temperature relatives of hyperthermophiles. *Proc. Natl. Acad. Sci. U.S.A.* **97**, 14421–14426.

Schouten S., Hopmans E. C., Schefuß E. and Sinninghe Damsté J. S. (2002) Distributional variations in marine crenarchaeotal membrane lipids: A new tool for reconstructing ancient sea water temperatures? *Earth. Planet. Sci. Lett.* **204**, 265–274.

Schouten S., Hopmans E. C., Forster A., van Breugel Y., Kuypers M. M. M. and Sinninghe Damsté J. S. (2003) Extremely high sea-surface temperatures at low latitudes during the middle Cretaceous as revealed by archaeal membrane lipids. *Geology* **31**, 1069–1072.

Schouten S., Forster A., Panato E. and Sinninghe Damsté J. S. (2007a) Towards the calibration of the TEX$_{86}$ paleothermometer in ancient green house worlds. *Org. Geochem.* **38**, 1537–1546.

Schouten S., Huguet C., Hopmans E. C., Kienhuis M. and Sinninghe Damsté J. S. (2007b) Analytical Methodology for TEX86 Paleothermometry by High-Performance Liquid Chromatography/Atmospheric Pressure Chemical Ionization-Mass Spectrometry. *Anal. Chem.* **79**, 2940–2944.

Schouten S., Pitcher A., Hopmans E. C., Villanueva L., van Bleijswijk J. and Sinninghe Damsté J. S. (2012) Intact polar and core glycerol dibiphytanyl glycerol tetraether lipids in the Arabian Sea oxygen minimum zone: I. Selective preservation and degradation in the water column and consequences for the TEX$_{86}$. *Geochim. Cosmochim. Acta* **98**, 228–243.

Schouten S., Hopmans E. C. and Sinninghe Damsté J. S. (2013) The organic geochemistry of glycerol dialkyl glycerol tetraether lipids: A review. *Org. Geochem.* **54**, 19–61.

Schouten S., Hopmans E. C., Rosell-Melé A., Pearson A., Adam P., Bauersachs T., Bard E., Bernasconi S. M., Bianchi T. S., Brocks J. J., Carlson L. T., Castañeda I. S., Derenne S., Selver A. D., Dutta K., Eglinton T., Fosse C., Galy V., Grice K., Hinrichs K.-U., Huang Y., Huguet A., Huguet C., Hurley S., Ingalls A., Jia G., Keely B., Knappy C., Kondo M., Krishnan S., Lincoln S., Lipp J., Mangelsdorf K., Martínez-García A., Ménot G., Mets A., Mollenhauer G., Ohkouchi N., Ossebaar J., Pagani M., Pancost R. D., Pearson E. J., Peterse F., Reichart G.-J., Schaeffer P., Schmitt G., Schwark L., Shah S. R., Smith R. W., Smittenberg R. H., Summons R. E., Takano Y., Talbot H. M., Taylor K. W. R., Tarozo R., Uchida M., van Dongen B. E., van Mooy B. A. S., Wang J., Warren C., Weijers J. W. H., Werne J. P., Woltering M., Xie S., Yamamoto M., Yang H., Zhang C. L., Zhang Y., Zhao M. and Sinninghe Damsté J. S. (2014) An interlaboratory study of TEX$_{86}$ and BIT analysis of sediments, extracts, and standard mixtures. *Geochem. Geophys. Geosyst.* **14**, 5263–5285.

Shah S. R., Mollenhauer G., Ohkouchi N., Eglinton T. I. and Pearson A. (2008) Origins of archaeal tetraether lipids in sediments: Insights from radiocarbon analysis. *Geochim. Cosmochim. Acta* **72**, 4577–4594.

Sinninghe Damsté J. S., Hopmans E. C., Schouten S., van Duin A. C. T. and Geenevasen J. A. J. (2002) Crenarchaeol: The characteristic core glycerol dibiphytanyl glycerol tetraether membrane lipid of cosmopolitan pelagic crenarchaeota. *J. Lipid Res.* **43**, 1641–1651.

Sinninghe Damsté J. S., Rijpstra W. I. C., Hopmans E. C., Jung M.-Y., Kim J.-G., Rhee S.-K., Stieglmeier M. and Schleper C. (2012) Intact polar and core glycerol dibiphytanyl glycerol tetraether lipids of Group I. 1a and I.1b Thaumarchaeota in soil. *Appl. Environ. Microbiol.* **78**, 6866–6874.

Sintes E., Bergauer K., De Corte D., Yokokawa T. and Herndl G. J. (2012) Archaeal amoA gene diversity points to distinct biogeography of ammonia-oxidizing Crenarchaeota in the ocean. *Environ. Microbiol.*. http://dx.doi.org/10.1111/j.1462-2920.2012.02801.x.

Smittenberg R. H., Hopmans E. C., Schouten S., Hayes J. M., Eglinton T. I. and Sinninghe Damsté J. S. (2004) Compound-specific radiocarbon dating of the varved Holocene sedimentary record of Saanich Inlet, Canada. *Paleoceanography* **19**, PA2012, 2003PA000927.

Spang A., Hatzenpichler R., Brochier-Armanet C., Rattei T., Tischler P., Spieck E., Streit W., Stahl D. A., Wagner M. and Schleper C. (2010) Distinct gene set in two different lineages of ammoniaoxidizing archaea supports the phylum Thaumarchaeota. *Trends Microbiol.* **18**, 331–340.

Taylor K. W. R., Huber M., Hollis C. J., Hernandez-Sanchez M. T. and Pancost R. D. (2013) Re-evaluating modern and Palaeogene GDGT distributions: Implications for SST reconstructions. *Global Planet. Change* **108**, 158–174.

Tesi T., Miserocchi S., Goñi M. A., Turchetto M., Langone L., De Lazzari A., Albertazzi S. and Correggiari A. (2011) Influence of distributary channels on sediment and organic matter supply in event-dominated coastal margins: The Po prodelta as a study case. *Biogeosciences* **8**, 365–385.

Tierney J. E. and Tingley M. P. (2014) A Bayesian, spatially-varying calibration model for the TEX$_{86}$ proxy. *Geochim. Cosmochim. Acta* **127**, 83–106.

Tourna M., Stieglmeier M., Spang A., Könneke M., Schintlmeister A., Urich T., Engel M., Schloter M., Wagner M., Richter A. and Schleper C. (2011) *Nitrososphaera viennensis*, an ammonia oxidizing archaeon from soil. *Proc. Natl. Acad. Sci. U.S.A.* **108**, 8420–8425.

Trommer G., Sicca M., van der Meer M. T. J., Schouten S., Sinninghe Damsté J. S., Schulz H., Hemleben C. and Kucera M. (2009) Distribution of Crenarchaeotal tetraether membrane lipids in surface sediments from the Red Sea. *Org. Geochem.* **40**, 724–731.

Villanueva L., Schouten S. and Sinninghe Damsté J. S. (2014) Depth-related distribution of a key gene of the tetraether lipid biosynthetic pathway in marine Thaumarchaeota. *Environ. Microbiol.*. http://dx.doi.org/10.1111/1462-2920.12508.

Weijers J. W. H., Schouten S., Spaargaren O. C. and Sinninghe Damsté J. S. (2006) Occurrence and distribution of tetraether membrane lipids in soils: Implications for the use of the TEX$_{86}$ proxy and the BIT index. *Org. Geochem.* **37**, 1680–1693.

Wuchter C., Schouten S., Boschker H. T. S. and Sinninghe Damsté J. S. (2003) Bicarbonate uptake by marine crenarchaeota. *FEMS Microbiol. Lett.* **219**, 203–207.

Wuchter C., Schouten S., Coolen M. J. L. and Sinninghe Damsté J. S. (2004) Temperature-dependent variation in the distribution of tetraether membrane lipids of marine Crenarchaeota: Implications for TEX$_{86}$ paleothermometry. *Paleoceanography* **19**. http://dx.doi.org/10.1029/2004PA001041.

Wuchter C., Abbas B., Coolen M. J. L., Herfort L., Timmers P., Strous M., van Bleijswijk J., Teira E., Herndl G. J., Middelburg J. J., Schouten S. and Sinninghe Damsté J. S. (2006) Archaeal nitrification in the ocean. *Proc. Natl. Acad. Sci. U.S.A.* **103**, 12317–12322.

Yakimov M. M., La Cono V., Smedile F., DeLuca T. H., Juárez S., Ciordia S., Fernández M., Pablo Albar J., Ferrer M., Golyshin P. N. and Giuliano L. (2011) Contribution of crenarchaeal autotrophic ammonia oxidizers to the dark primary production in Tyrrhenian deep waters (Central Mediterranean Sea). *ISME J.* **5**, 945–961.

Zell C., Kim J.-H., Abril G., Sobrinho R. L., Dorhout D., Moreira-Turcq P. and Sinninghe Damsté J. S. (2013a) Impact of seasonal hydrological variation on the distributions of tetraether membrane lipids along the Amazon River in the central Amazon basin: Implications for the MBT/CBT paleothermometer and the BIT index. *Front. Microbiol.* **4**. http://dx.doi.org/10.3389/fmicb.2013.00228.

Zell C., Kim J.-H., Moreira-Turcq P., Abril G., Hopmans E. C., Bonnet M.-P., Sobrinho R. L. and Sinninghe Damsté J. S. (2013b) Disentangling the origins of branched tetraether lipids and crenarchaeol in the lower Amazon River: Implications for GDGT-based proxies. *Limnol. Oceanogr.* **58**, 343–353.

Associate editor: Elizabeth Ann Canuel